AN INVESTIGATION OF THE INFLUENCE OF FUSELAGE ELASTICITY ON THE PITCHING MOTION OF A CONTROLLED MISSILE

Thesis by

Harry Nelson Upthegrove

In Partial Fulfillment of the Requirements

for the Degree of

Doctor of Philosophy

California Institute of Technology

Pasadena, California

1954

PREFACE

Shortly after his arrival at the California Institute of Technology, the author became acquainted with the large-scale, general-purpose electric analog computer. The decision was made at that time to direct his research program toward a project involving the application of such a computer in the study of feedback control systems. Construction of a smaller electric analog computer in the Servomechanisms Laboratory at the California Institute of Technology provided additional facilities, and, under the direction of Dr. G. D. McCann, this investigation was undertaken.

The help and encouragement given by Dr. G. D. McCann and Dr. C. H. Wilts, who directly supervised the research, are acknowledged with sincere appreciation. The author is also indebted to Dr. R. H. MacNeal and B. N. Locanthi who provided advice and assistance whenever called upon.

To his wife, without whose aid and understanding this thesis could not have been completed, the author is especially grateful.

ABSTRACT

This thesis describes an investigation of the effects of elastic deformation on the performance of a guided missile type of aircraft. An imaginary typical missile is selected, and an electric model is devised to represent the missile with its associated aerodynamic forces and control functions. The results of measurements on this model are presented in the form of oscillographs, and their significance is discussed.

It is determined that elasticity effects can rarely be ignored, and that improvement in missile and control system performance will probably require more rather than less consideration of elastic deformation of the aircraft structure.

TABLE OF CONTENTS

TABLE OF SYMBOLS AND UNITS and STATEMENT OF REFERENCE CONDITIONS

a, b, — Scale factors relating the electrical and mechanical quantities.

$$a = \frac{a_o V_o}{V} \qquad b = \frac{b_o V_o}{V}$$

a_o, b_o — Reference values of a and b.

A — In general, the gain of an amplifier.

A2 — The gain of the R4 channel through amplifier A2.

A5 — The gain of the R11 channel through amplifier A5.

c — Chord length of an aerodynamic surface.

D — Distance between the forward aerodynamic surface and the tail aerodynamic surface.

E_α — Voltage in the electric model corresponding to rate of change of angle of attack on an aerodynamic surface, equal to E_θ at the point of attachment of the airfoil to the fuselage.

$E_{\alpha b}$ — Voltage output of the control system model, representing angular positioning of the control surface.

$E_{\alpha c}$ — Excitation voltage, representing an arbitrary angular displacement of the control surface.

$E_{\alpha d}$ — Voltage output of the downwash delay line, representing the equivalent additional angle of attack introduced at the tail surface by downwash.

E_h	Voltage in the electric model fuselage displacement circuit, representing displacement velocity.
E_θ	Voltage in the electric model fuselage slope circuit, representing pitching angular velocity.
$E_{\theta s}$	Voltage in the electric model corresponding to $p\theta_s$.
EI	Young's Modulus - moment of inertia product for an element of the fuselage beam.
$f_{1,2,3}$	First, second, and third bending mode frequencies of the fuselage beam.
G	The conductance, or output current to input voltage ratio, of an amplifier used as a current generator.
G(p)	Transfer function of the combined missile fuselage and aerodynamic loading.
h	Vertical displacement of an aerodynamic surface or of a point on the missile fuselage, positive for downward displacement.
h	Altitude of flight in feet.
H(p)	Frequency dependent portion of the control system transfer function.
i_α	Electric model equivalent of moment on an airfoil.
i_h	Electric model equivalent of lift on an airfoil.
i_m	Electric model equivalent of moment on a beam.
i_s	Electric model equivalent of shear force in a beam.

k	Ratio of the additional effective tail surface angle of attack due to downwash to the angle of attack on the forward aerodynamic surface.
K	The portion of the control system transfer function which is independent of frequency.
K	Arbitrary scale factor relating the energy levels of the mechanical and electrical systems.
l	Length of the fuselage beam.
L	Lift force acting on an aerodynamic surface, positive for downward force.
m	Mass per unit length of the fuselage beam.
M	Moment on an airfoil or moment in the fuselage beam.
N	Time scale ratio. $N = \frac{N_o V_o}{V}$
p	Differential operator $\frac{d}{dt}$ in mechanical system time.
$\bar{p}$	Differential operator $\frac{d}{d\bar{t}}$ in electric model time.
PP	Used with a station number to indicate the point on the fuselage at which an oscillographic measurement was made.
q	$\frac{1}{2}\rho V^2$
r	Coefficient of the rate term in the control system transfer function.
S	Shear force in the fuselage beam.
S	Area of an aerodynamic surface.

SP	Used with a station number to indicate the location of the feedback control system sensing point, such as SP50.
t	Time in the mechanical system.
$\bar{t}$	Time in the electric model.
V	Air stream velocity or velocity of flight.
V_o	Reference velocity.
W	Total weight of the missile.
x	Distance along the fuselage beam, measured from the nose.
Δx	Increment in x between cells in the finite difference representation of a beam.
X_1	Location of center of lift of the forward aerodynamic surface.
X_2	Location of center of lift of the tail aerodynamic surface.
α	Angular position of an aerodynamic surface, positive for leading edge up.
α_b	Control surface angular position introduced by the feedback control system.
θ	Slope angle at any point on the missile fuselage, positive for nose up.
θ_s	Slope angle of the fuselage at the sensing point for the control system.
ρ	Density of the air at the altitude of flight.
$\tau 1, \tau 2$	Time delays in the control system.

Subscript 1 Quantity in question applies to the forward aerodynamic surface.

Subscript 2 Quantity in question applies to the tail aerodynamic surface.

Subscript n Used to indicate cell number in the finite difference representation of a beam.

Subscript o Indicates the particular value of the quantity in question which is associated with the reference conditions.

$\underline{100}$ x coordinate of any point along the fuselage used as a station number on the electric circuit diagrams.

Unless otherwise stated the units used throughout this study are

Time.....seconds

Force.....pounds

Length.....inches

Voltage.....volts

Current.....amperes

Resistance.....ohms

Inductance.....henries

Capacitance.....farads

Capacitance
Numerical Values...microfarads

For ease in presenting and discussing the results a particular combination of scale factors, fuselage constants, aerodynamics, and control parameters is defined as the reference condition. The numerical values associated with this condition are summarized here for the convenience of the reader. It should also be noted that, unless otherwise indicated, all oscillographs present the behavior of E_θ at station 50.

Aerodynamics

$V = V_o = 995$ feet per second

$h = 30{,}000$ feet

$X_1 = 47.5$ inches

$X_2 = 137.5$ inches

$c_1 = 10$ inches

$c_2 = 12.5$ inches

$S_1 = 200$ square inches

$S_2 = 375$ square inches

$k = 0.16$

Fuselage Constants

The fuselage is a uniform beam.

$W = 750$ pounds

$f_1 = 15.0$ cycles per second

Control Parameters

$K = 0.90$

$r = 0.3$

$\tau 1 = 0.1$ seconds

$\tau 2 = 0.1$ seconds

SP = Station 50

Scale Factors

$N = N_o = 60$

$a = a_o = .035$

$b = b_o = .0014$

I

INTRODUCTION

The publicity given the development of new weapons systems depending upon automatically controlled aircraft or guided missiles has emphasized the need for more detailed knowledge of the behavior of such missiles in flight. The design of a control system for an aircraft is a complex task involving problems of aerodynamics and elasticity as well as the usual electrical and mechanical considerations. In dealing with a self-contained, pilotless missile the designer is faced with additional restrictions due to the absence of any provision for human judgment or correction. An obvious simplification of the problem is to treat the missile structurally as a rigid body. With conservative design this approximation probably has little effect upon the final result. As system requirements are made higher and tighter, however, it becomes increasingly difficult to maintain any reserve of performance; the design becomes marginal. Consequently, it is significantly more important to eliminate as far as possible the uncertainties in the design of missile control systems. The rigid body assumption is therefore untenable without better information about the limits of the region within which it is applicable and the amount of error which it introduces outside that region.

The Analysis Laboratory of the California Institute of Technology has pioneered in the application of the electric analog computer to the study of elastic structures subjected to aerodynamic forces, including work on the specific problem set forth in the preceding paragraph. (Ref. 1) The author's objective in carrying out this research was to add to the existing knowledge of the effect of fuselage elasticity upon missile control systems and to gain some understanding of its influence upon the effects of variations in control system parameters.

II

SELECTION OF A MISSILE

At the beginning of an investigation of this nature one must choose a basic system which will serve as a starting point for the ensuing program. A study involving missile control systems could well begin with a particular missile already in military service. This approach would offer the advantageous possibility of comparing results with measured performance data. It would have been necessary, however, to conduct the research under the restrictions of security classification; therefore, such an approach was not considered. In addition it was desired to direct the research along general rather than specific lines. As a result of these considerations an imaginary typical missile was chosen. The particular characteristics of this missile were determined after discussions with Dr. H. J. Stewart and Dr. C. H. Wilts concerning the aerodynamic design and the control requirements of missiles in general.

Figure 1 is an approximate planform of the selected missile. The fuselage is represented by a cylindrical structure 10 inches in diameter and 150 inches long. The structural rigidity of the fuselage is specified by stating that the frequency of its first bending mode is 15 cycles per

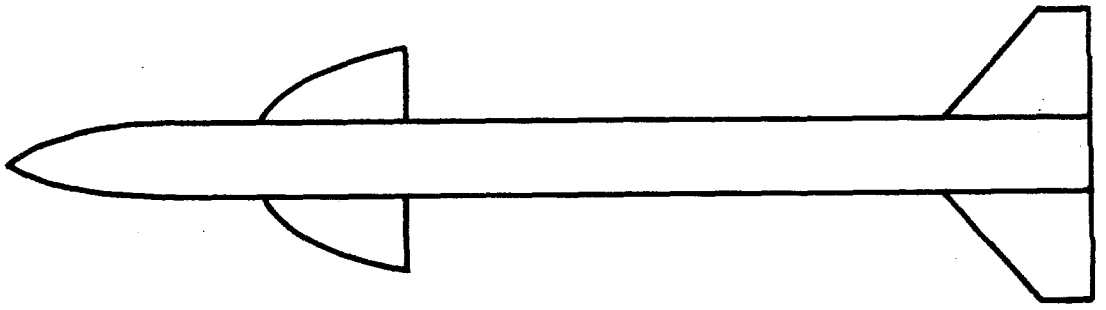

Planform of the Missile
Figure 1

second. The 750 pound total weight of the missile is assumed to be uniformly distributed over the length of the fuselage, giving a linear mass density, m, of 0.01295 $lbs\text{-}sec^2 / in^2$.

The missile has two aerodynamic surfaces, a forward, or control, surface located 47.5 inches from the nose, and a tail surface 137.5 inches from the nose. The mean chord length and area of the forward surface are 10 inches and 200 square inches; for the tail surface they are 12.5 inches and 375 square inches. The small size and large rigidity of the aerodynamic surfaces justify the assumption that their elastic deformation is of no significance; therefore, they are treated as if they are infinitely rigid. The aerodynamic behavior of the missile is also a function of altitude and velocity of flight. According to information obtained from Dr. H. J. Stewart, sea-level to 60,000 feet is an appropriate range of altitude, and velocities may be expected to vary from zero

to Mach 2.5. For the reference condition the flight velocity and altitude are Mach 1.0 and 30,000 feet. The effect of downwash from the forward surface on the lift at the tail surface depends to a large extent upon the ratio of the two spans. In practice the designer usually attempts to minimize this effect, so a fairly low value, k = 0.16, is chosen for the reference condition.

The pitch control system chosen for the missile is a relatively simple one. It can be described as a second order system providing position and rate feedback with two time delays. The transfer function of the control system is

$$KH(p) = K \frac{(1 + rp)}{(1 + \tau 1p)(1 + \tau 2p)} . \qquad (1)$$

Both time delays are initially set at 0.1 seconds; the gain and rate coefficient have the values K = 0.9 and r = 0.3.

It is obvious that the missile described above is not a complete, real missile. The fuselage of an actual missile is certainly not uniform over its length; it may be a series of almost rigid sections joined by short connecting sections of varying flexibility. The author does not believe, however, that possible departures from the uniform fuselage will invalidate the results; the overall nature of the structure, as specified by its weight and first bending mode frequency, is more significant than its detailed construction. The aerodynamic and control parameters of this missile are

incomplete, since they are sufficient only to determine the longitudinal pitching behavior of the missile. Only this much of the missile is specified, and the study is restricted to the pitching motion, because it is believed that the most serious effects of elastic deformation will be found therein. The reader will also note that, as detailed in Appendices A, B, and C, the system has been simplified whenever possible in order to obtain a straightforward representation of general missile characteristics which can be readily studied by means of an electric model requiring an easily obtainable number of circuit elements.

III

DESCRIPTION OF THE ELECTRIC MODEL

The electric model of the missile system is made up of five circuits representing the fuselage beam, the forward aerodynamic effects, the tail aerodynamic effects, downwash effects, and the pitch control system. A block diagram of the electric model is shown in Figure 2, and a complete circuit diagram is presented in Figure 71.

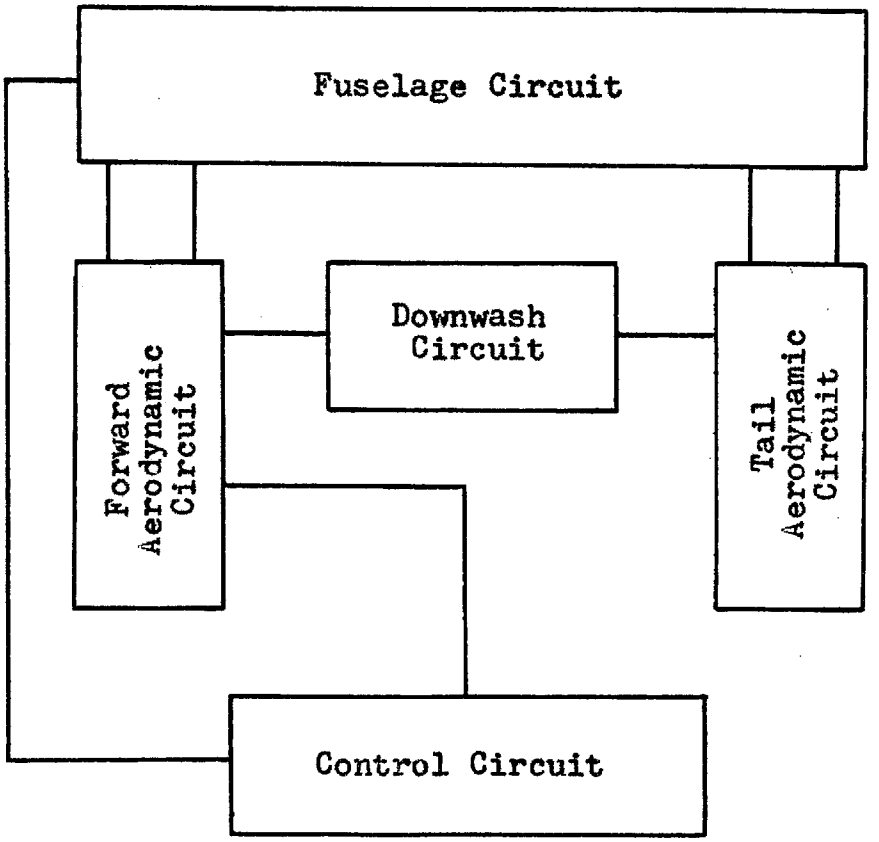

Block Diagram of Electric Model
Figure 2

The missile fuselage, treated as a free-free beam, is represented by the six cell circuit shown in Figure 3. The derivation of the circuit and expressions for determining the values of the circuit elements are included in Appendix A.

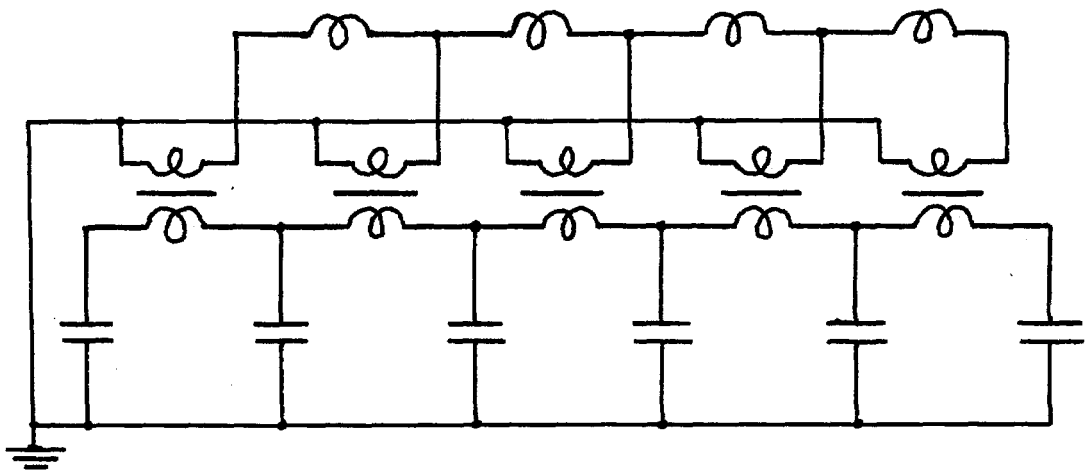

Missile Fuselage Circuit
Figure 3

Voltages measured at the inductor nodes represent pitch angle velocities at the corresponding points on the fuselage. Vertical displacement velocities are represented by voltages at the condenser nodes. The transformers are treated as distributed elements, so that turns along the winding are analogous to distance increments along the missile. Thus, a lift force acting at a particular position on the missile is represented by a current inserted into the circuit at the appropriate transformer tap.

Figure 4 is a schematic diagram of the aerodynamic circuit employed by the author. Two circuits of this type are required, one for each of the aerodynamic surfaces. An additional network connecting these two circuits is needed to represent the downwash coupling between the airfoils.

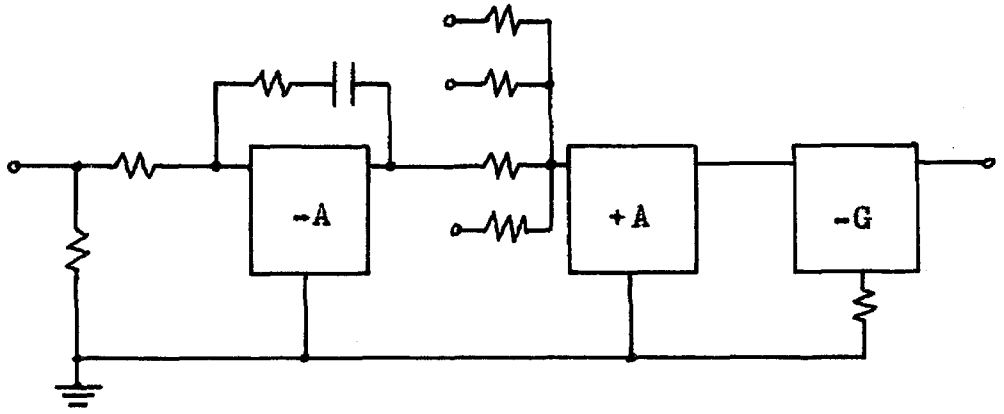

Aerodynamic Circuit
Figure 4

Neglecting the aerodynamic lag terms, thereby letting Theodorsen's Function equal unity, and defining the airfoil position parameters, X_1 and X_2, as the locations of the centers of lift, the aerodynamic equations (Ref. 2) can be written in operational form as

$$L = -2\pi qS \left\{ \left(\frac{c}{4V} + \frac{x_2}{V} \right) p\alpha + \frac{ph}{V} + \alpha \right\} \qquad (2)$$

and

$$Mea = -2\pi qS \left(\frac{c^2}{8V}\right) p\,\alpha\,. \qquad (3)$$

The circuit of Figure 4 is derived from these simplified equations. A detailed description with circuit element values may be found in Appendix B. The input to the aerodynamic circuit is the fuselage slope voltage at the point of attachment of the airfoil. Since the airfoils are small compared to the fuselage, there is negligible variation in the fuselage slope angle over the chord; thus, the center of lift coordinate may be used to define the point of attachment as well as the point at which the lift current output of the aerodynamic circuit is inserted. The downwash circuit is shown in Figure 5. It provides for the introduction of a suitably delayed voltage proportional to lift on the forward airfoil into the tail aerodynamic circuit to represent the increment in the tail surface angle of attack due to downwash. The derivation of circuit element values for the downwash model is presented in Appendix B.

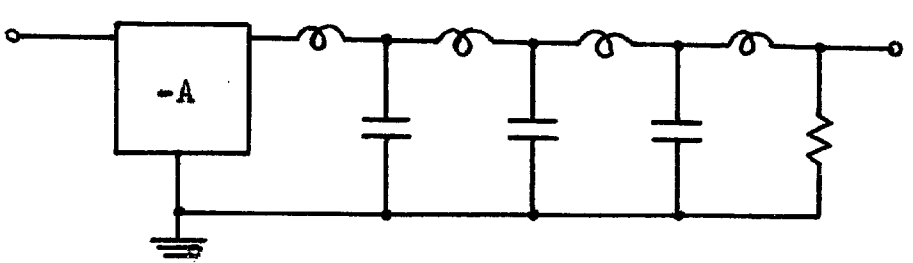

Downwash Circuit
Figure 5

The fifth circuit of the electric model represents the pitch control system of the missile. Appendix C contains a detailed description of the circuit and expressions for determining circuit element values, while Figure 6 shows a simple schematic diagram of the circuit.

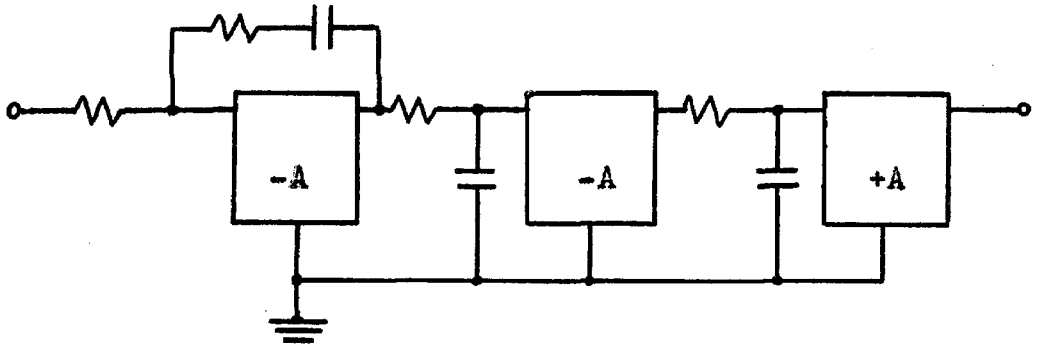

Control Circuit
Figure 6

The control circuit receives an input voltage, representing the output of a slope angle sensing device, from one of the nodes in the slope circuit of the electric fuselage model. The output voltage of the control circuit is connected to the forward aerodynamic circuit where it represents a corresponding change in the control surface angle of attack.

IV

TESTING THE ELECTRIC MODEL

In order to establish the accuracy of the electric model prior to beginning transient studies of the complete system, two sets of tests were carried out on portions of the circuit.

The reference-condition fuselage circuit was assembled first, and a mode study was performed. The measured mode shape data is superimposed on plots of theoretical mode shapes in Appendix D. For the first and second modes the measured points fall directly on the calculated curves, and the maximum frequency error is five percent. For the third and higher modes, however, agreement between theory and measured data deteriorates rapidly. This is to be expected since the fuselage beam circuit has only six cells, and the error in the finite difference analogy varies inversely as the number of cells. The higher modes of the fuselage beam were not expected to play a significant part in the determination of system behavior, so, on the basis of the mode study, the six-cell fuselage model was judged to adequately represent the fuselage for this investigation. The observed behavior of the complete system confirms the unimportance of the higher modes.

When the fuselage and aerodynamic circuits were combined, it was possible to make steady state measurements and determine the transfer function between control surface angle and fuselage slope angle for the uncontrolled system. The correctness of the aerodynamic circuits was verified by simple transmission measurements, so the transfer function measurements were performed on a circuit which was known to be a valid representation of both the fuselage and the aerodynamic forces. The transfer function of the proposed control system is described precisely by inserting numerical values in the equation for $KH(j\omega)$ (Eqn. 1). This information may be combined with the measured fuselage-aerodynamics transfer function $G(j\omega)$ to obtain the complete open-loop transfer function of the system. Some predictions may then be made concerning the stability of the closed-loop system. This procedure was carried out for several systems and is described in detail for the reference condition in Appendix E. The results are given there in the form of gain and phase plots and an oscillograph of the observed closed-loop behavior. From the plots it was determined that the closed-loop system should be marginally stable at 2.0 cycles per second with $K = 0.84$. The oscillograph (Fig. 70) shows the behavior of the complete circuit with $K = 0.90$; marginal

stability occurs at 1.95 cycles per second. This agreement is well within the limits of accumulated measurement error, and since similar agreement was obtained for other fuselage-control combinations, these results verify the configuration and connections of the control circuit.

V

TRANSIENT STUDY PROGRAM

In the early stages of this research, data was collected in the form of steady state measurements leading to transfer function plots such as those discussed in Section IV. If similar plots were available for a large variety of fuselage and aerodynamic parameters, the control system designer could presumably use them to determine an optimum design; however, an inordinate amount of labor would be involved. Furthermore, the time and effort required to obtain a single transfer function mitigates against the application of this method to a problem requiring a large number of answers. While the system studied is not complex in the ordinary sense, its overall behavior is dependent upon a large number of variable parameters. Thus, a great number of cases, or combinations of parameters, must be investigated. Therefore, the steady state approach was discarded in favor of oscillographic transient studies.

The system was excited by an arbitrary sudden change in the control surface angle of attack represented in the electric model by a square pulse of voltage, E_{α_c}, inserted in the control surface aerodynamic circuit. This forcing function is shown in Figure 7. The width of the

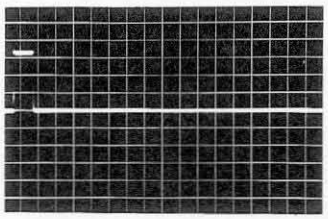

1sec.= 4.3 sqs.
Forcing Function
Figure 7

pulse was variable, so that it was possible to emphasize the excitation of one root or mode in preference to another. The response of the system was recorded by photographing the face of an oscilloscope connected to various points in the fuselage circuit. The assumption of infinitely rigid airfoils made it unnecessary to observe their behavior independently of the fuselage. The behavior of fuselage vertical displacement voltages was recorded for the sake of completeness in a few cases, but in general, the oscillographs present fuselage slope angle voltages. Thus, the frequency and damping of the longitudinal pitching motion roots may be scaled directly from the photographs.

The test program was not laid out entirely in advance, but developed in the directions indicated by the data as it was obtained. The variables affecting system performance are listed below.

1. Fuselage.
    a. Weight.
    b. Rigidity.
    c. Uniformity.

2. Aerodynamics.
    a. Velocity of flight.
    b. Altitude of flight.
    c. Size of airfoils.
    d. Location of airfoils.
    e. Downwash coefficient.
3. Control.
    a. Location of the feedback sensing device.
    b. Values of the constants in KH(p).

The primary objective of this research was to determine the effects of variations in the elastic behavior of the fuselage, so item 1b is the variable of first importance. The location of the feedback sensing device is the parameter which largely determines the extent to which fuselage elasticity will affect overall system performance, so item 3a is the second important variable. Variations in the aerodynamic parameters were not, in general, examined for their own sake, but the extent to which their effects depended upon fuselage elasticity was investigated. The constants in KH(p) were treated as independent parameters subject within limits to the designer's control in attempting to achieve a satisfactory control system. With this emphasis on fuselage stiffness and sensing point location, measurements were begun on the combined fuselage and

aerodynamic circuits without the control circuit. These measurements, discussed in Section VI-A, established the basic nature of the effects of variations in fuselage structure and position along the missile. The control system described as part of the reference condition in Section II was then added to complete the system. The value of K_o, reference condition control system gain, was chosen to give marginal stability so as to achieve maximum sensitivity to variations in the system. Section VI-B describes the behavior of this particular system. The control system was modified to raise the system frequency and more extensive measurements were made. The modified control will be referred to as the K_1H_1 control; the oscillographs in Section VI-C present the K_1H_1 system. The K_1H_1 control has 0.05 second time delays, about the limit of ordinary good control devices, but it still requires an unusually high derivative term to increase the system frequency appreciably. The K_2H_2 control is a hypothetical faster system with a lower rate coefficient. Sections VI-D and VI-E describe this system with K_2 giving zero damping and K_3 providing 8 db of gain margin respectively.

Since there are a large number of oscillographs, some conventions have been adopted to simplify their display. Except where more data is provided for clarity, the only information given on the figures is that necessary to specify

how the conditions applying to each oscillograph differ from the reference conditions. Each caption includes the appropriate time scale plus any information which applies to all the oscillographs in that particular figure. Under each individual oscillograph will be found the additional variations appropriate to it alone. The abbreviations HFR and LFR indicate that the forcing function width was adjusted to emphasize the high or low frequency root respectively. The reference condition parameters are completely defined at the end of the TABLE OF SYMBOLS AND UNITS on pages ix and x. The most significant values may be restated by briefly describing the reference condition. The 750 pound missile, with a fuselage first bending mode frequency, f_1, of 15.0 cycles per second, is flying at Mach 1.0 at 30,000 feet. It has two airfoils located 47.5 and 137.5 inches from the nose; the downwash ratio is 0.16. A feedback signal is taken from a slope angle sensing device located at station 50 (SP50); the control is described by

$$K_o H_o(p) = 0.9 \frac{(1+0.3p)}{(1+0.1p)^2} . \qquad (5)$$

The behavior of the system is observed by examining the slope angle voltage in the fuselage circuit at station 50 (PP50).

Modifications in the control system are described by the equations

$$K_1 H_1(p) = 0.75 \frac{(1+0.9p)}{(1+0.05p)^2} , \qquad (6)$$

$$K_2H_2(p) = 10.4 \frac{(1+ 0.068p)}{(1 + 0.033p)(1 + 0.005p)} , \qquad (7)$$

and

$$K_3H_2(p) = 4.1 \frac{(1 + 0.068p)}{(1 + 0.033p)(1 + 0.005p)} . \qquad (8)$$

VI

DISCUSSION OF RESULTS

A. Behavior Without Control.

Basically the missile without control can be considered as a free-free beam with two vertical forces acting due to aerodynamic effects. A nose-up increase in the fuselage slope angle produces upward lift forces on both airfoils. The tail surface lift tends to reduce the nose-up angle, producing a stabilizing effect, while the lift on the forward surface is destabilizing. For small motions the frequency of this system will be determined by the ratio of restoring moment to angular displacement, or equivalent rotational spring constant, and the moment of inertia of the system about its center of gravity. Calculations for such a simple system give a frequency slightly less than one cycle per second. Any change which increases the moment due to the tail surface will increase the frequency, and additional moment due to the forward surface will lower the frequency.

The effect of varying the fuselage stiffness is demonstrated for three different positions on the fuselage in Figures 8 and 9. The fuselage starts out, at the top of Figure 8, infinitely rigid; its stiffness is reduced in five steps until, in the second row of Figure 9, the value of f_1 is only 4.7 cycles per second. This total variation

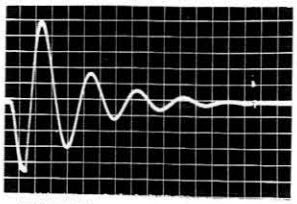

PP50 $f_1 = \infty$

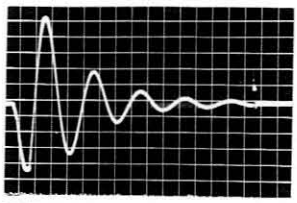

PP125 $f_1 = \infty$

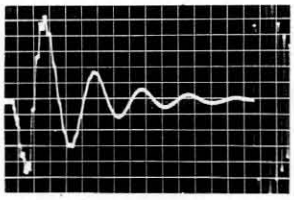

PP50 $f_1 = 15.0$

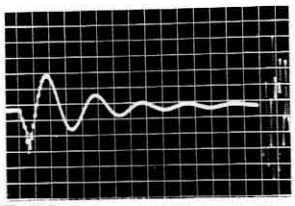

PP75 $f_1 = 15.0$

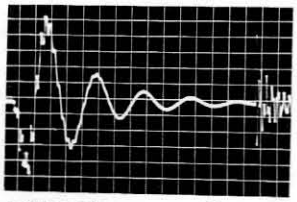

PP125 $f_1 = 15.0$

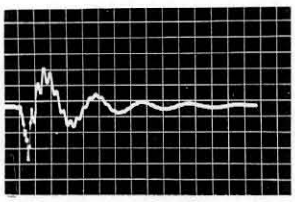

PP50 $f_1 = 10.6$

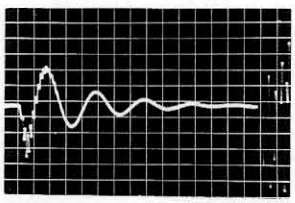

PP75 $f_1 = 10.6$

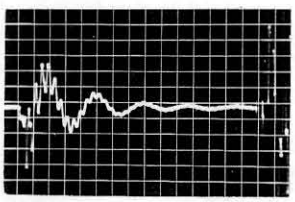

PP125 $f_1 = 10.6$

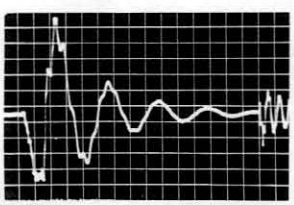

PP50 $f_1 = 7.5$

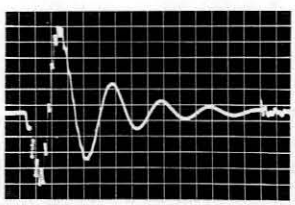

PP75 $f_1 = 7.5$

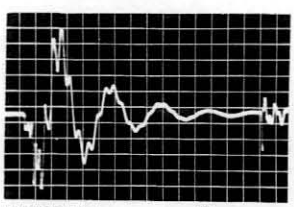

PP125 $f_1 = 7.5$

Variations in Fuselage Structure Without Control
1sec. = 4.2sqs. No Control

Figure 8

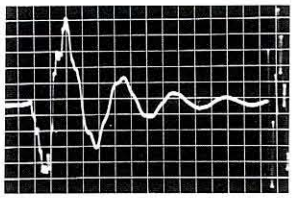

PP50 $f_1 = 5.3$

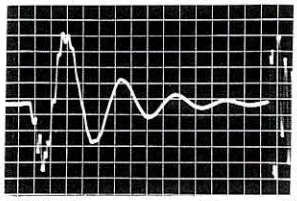

PP75 $f_1 = 5.3$

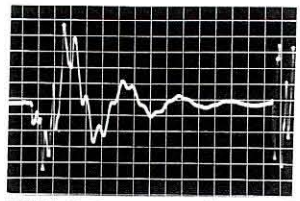

PP125 $f_1 = 5.3$

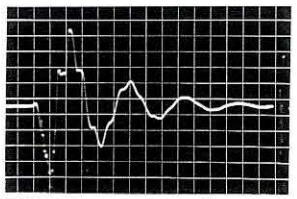

PP50 $f_1 = 4.7$

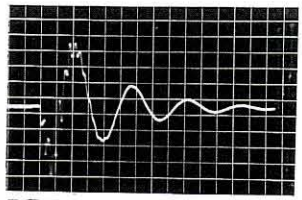

PP75 $f_1 = 4.7$

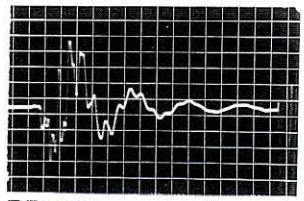

PP125 $f_1 = 4.7$

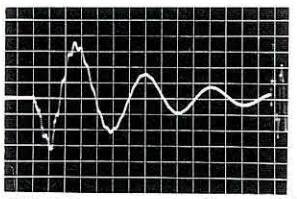

PP50 $f_1 = 10.6$
W = 1500

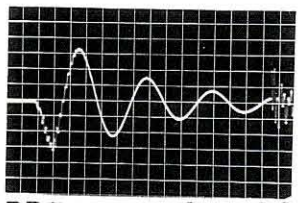

PP75 $f_1 = 10.6$
W = 1500

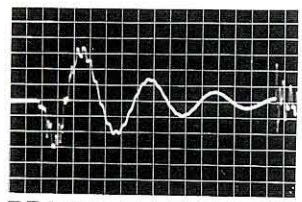

PP125 $f_1 = 10.6$
W = 1500

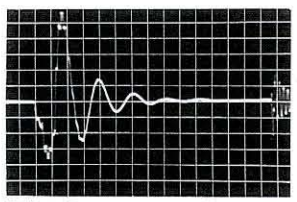

PP50 $f_1 = 21.2$
W = 375

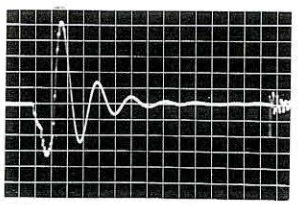

PP75 $f_1 = 21.2$
W = 375

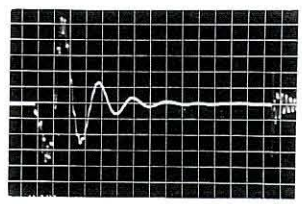

PP125 $f_1 = 21.2$
W = 375

Variations in Fuselage Structure Without Control
1sec. 4.2sqs. No Control

Figure 9

reduces the system frequency from 1.5cps to 1.2cps and has negligible effect upon the damping. The higher frequency root, which is present due to the bending modes of the beam in the non-rigid cases, varies from 12.5cps to 10.5cps with little change in the damping. Changing the nature of the fuselage by varying the weight, as shown in the bottom rows of Figure 9, has precisely the expected effect. Changing the weight by a factor of two in either direction multiplies the frequency by $\sqrt{2}$ or $1/\sqrt{2}$ as the weight and rotational moment of inertia are decreased or increased.

Variation in position along the fuselage changes the observed behavior very little, and does not affect the measured values of frequency and damping. It will be noted, however, that in every case the high frequency root is more prominent at the ends of the missile than it is in the center. This is definitely not true of the principal root. Remembering that the oscillographs record voltages which actually represent $p\theta$ at the point of measurement, these effects are readily explained by the slope mode shapes shown in Figure 10.

The behavior observed in Figures 8 and 9 is as expected for the uncontrolled system. The stable basic motion is that of the "fish-tailing", free-free, rigid beam with aerodynamic forces. As predicted it is affected directly by changes in the mass of the structure but

modified only slightly by increasing the flexibility. The variations in behavior observed at different points on the beam seem small, but their effects are amplified when the control system is added and the feedback loop closed.

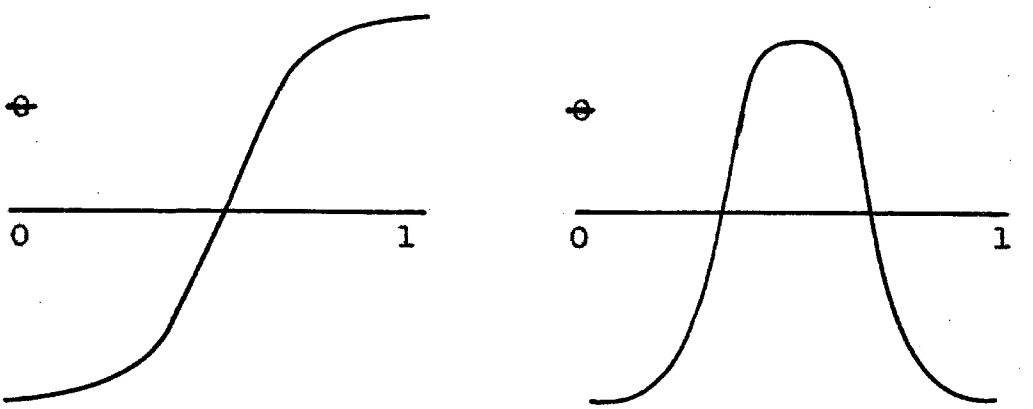

First Mode Second Mode

Slope Angle Mode Shapes
Figure 10

B. The Complete Reference Condition System.

The K_oH_o control was selected as a reasonable first approach to a good realistic control system. Its addition to the reference condition fuselage and aerodynamics increases the principal frequency of the system to 2.0 cycles per second. This is not enough to justify labeling it a good system, but it does provide some results of interest. Since the measurements on the uncontrolled system indicate that little information would be gained by shifting the measurement point along the fuselage, it is left at station 50 for most of the oscillographs. Figures 11 through 14 demonstrate the expected correlation between fuselage elasticity and the effect of changes in the location of the sensing device. The significant results of these observations are plotted in Figure 15. The quantity Δf is the change in frequency of the principal root, measured from the rigid case, while $\Delta\delta$ is the increment in damping, in percent per cycle, affected by moving the sensing point from station 25 to station 125. The last five pictures in Figure 14 show how the behavior of the two roots is linked. After shifting the sensing point to station 125 to pick up a larger amplitude high frequency signal, the two roots were examined selectively by adjusting the forcing function and measuring at the tail and midpoint of the fuselage. It is observed that, with $K = 2.0$, the high

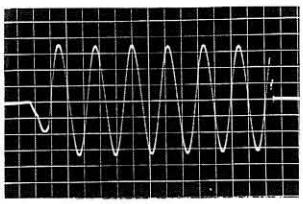

$f_1 = \infty$

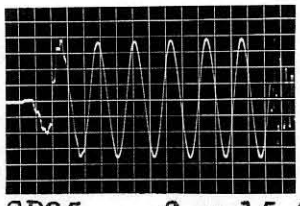

SP25 $f_1 = 15.0$

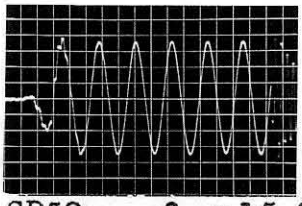

SP50 $f_1 = 15.0$

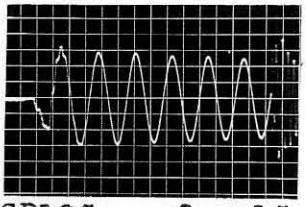

SP125 $f_1 = 15.0$

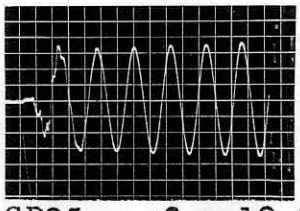

SP25 $f_1 = 10.6$

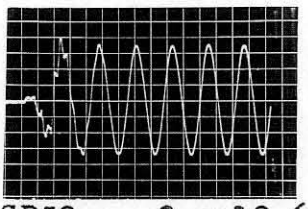

SP50 $f_1 = 10.6$

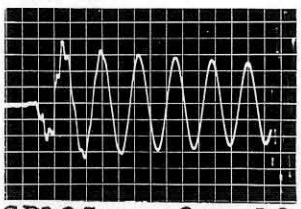

SP125 $f_1 = 10.6$

Varying Fuselage Elasticity
1sec. = 4.2sqs.

Figure 11

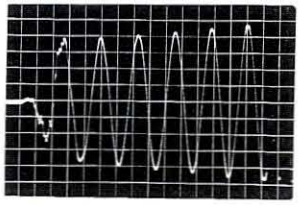

SP25

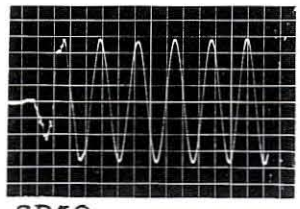

SP50

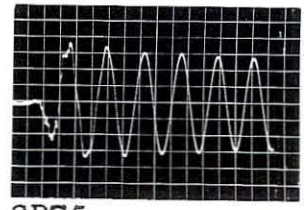

SP75

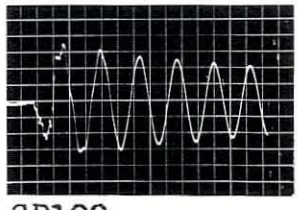

SP100

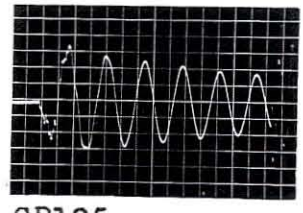

SP125

Varying Fuselage Elasticity
1sec. = 4.2sqs. f_1 = 7.5cps

Figure 12

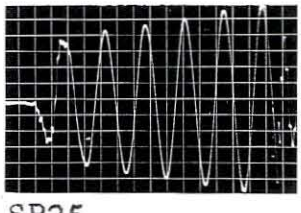

SP25

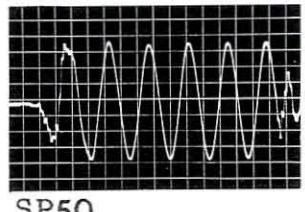

SP50

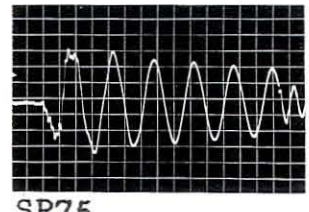

SP75

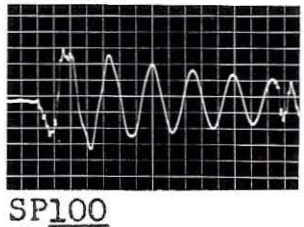

SP100

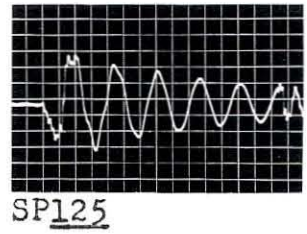

SP125

Varying Fuselage Elasticity
1sec. = 4.2sqs. f_1 = 5.3cps

Figure 13

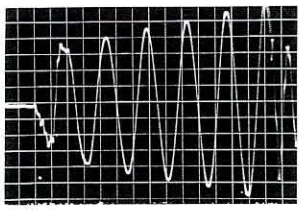

SP25

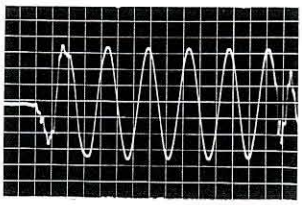

SP50

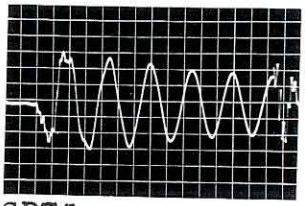

SP75

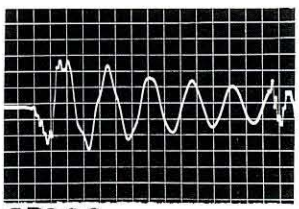

SP100

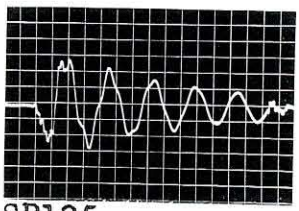

SP125

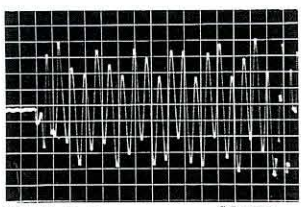

SP125 HFR
PP125 K = 2.0

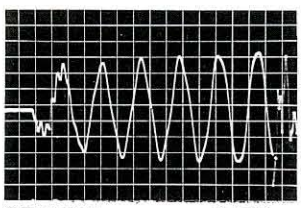

SP125 LFR
PP75 K = 2.0

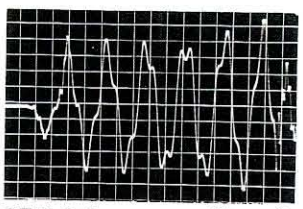

SP125 K = 2.0
PP50

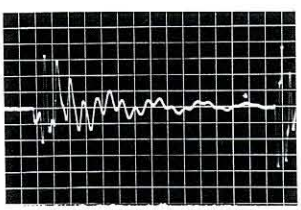

SP125 HFR
PP125 K = .64

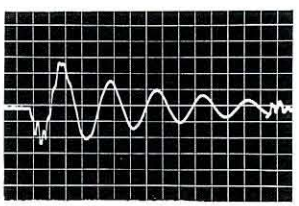

SP125 LFR
PP75 K = .64

Varying Fuselage Elasticity
1sec. = 4.2sqs. f_1 = 4.7cps

Figure 14

frequency root is marginally stable, while the low frequency root is slightly unstable. When the gain is reduced, as shown in the last two pictures, the high frequency root is damped less rapidly due to the location of the sensing point at the extreme end of the fuselage.

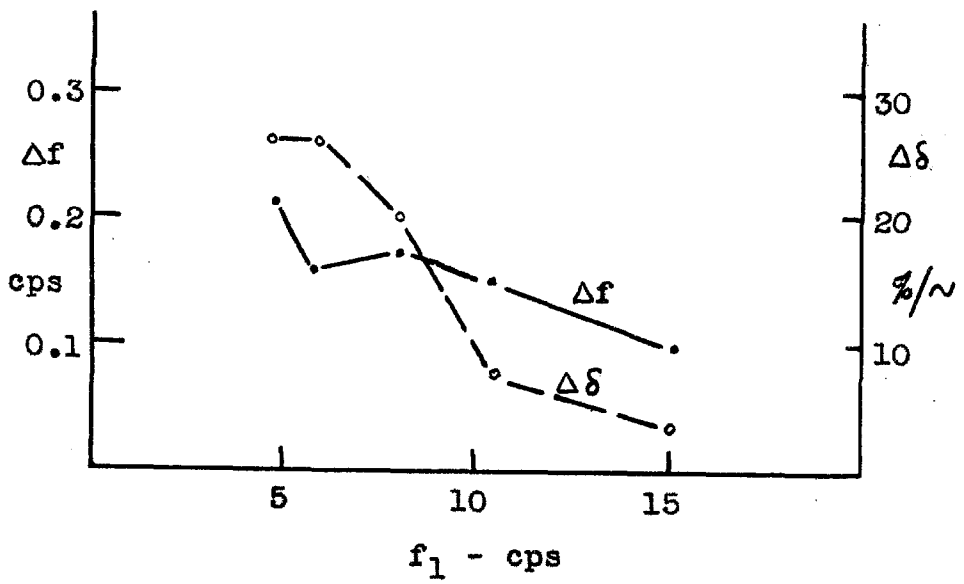

Effect of Varying Fuselage Elasticity
$K_o H_o$ Control
Figure 15

Before modifying the control system a brief examination was made of the effect of varying the downwash ratio. Figure 16 shows the results obtained with a fuselage beam having $f_1 = 7.5$cps. Since downwash reduces the effectiveness of the tail surface, it tends to destabilize

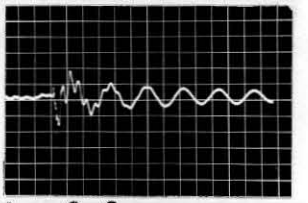

k = 0.0

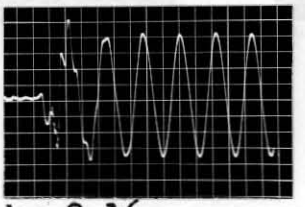

k = 0.16

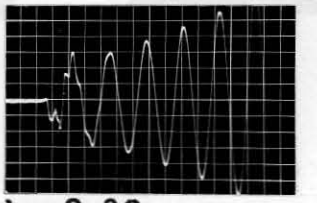

k = 0.32

Varying Downwash Ratio
1sec. = 4.2 sqs. f_1 = 7.5cps

Figure 16

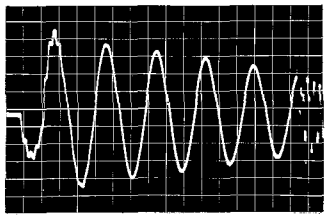

r = 0.0

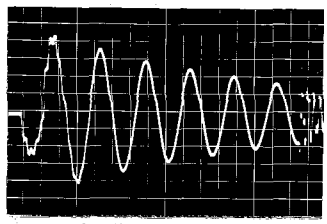

r = 0.1

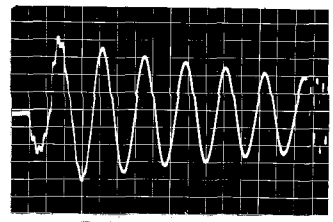

r = 0.2

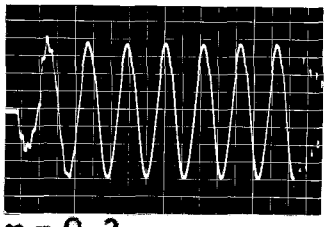

r = 0.3

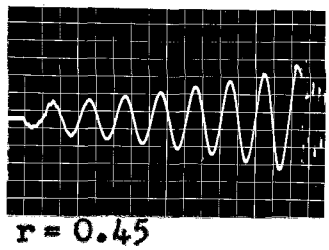

r = 0.45

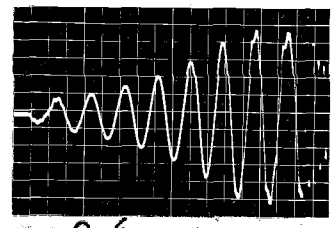

r = 0.6

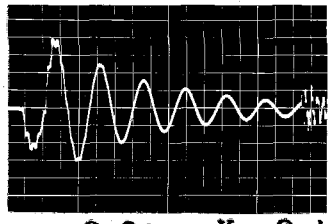

r = 0.3 K = 0.45

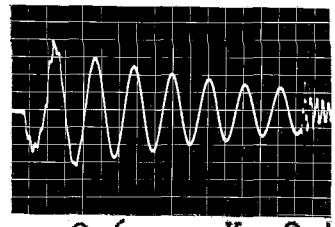

r = 0.6 K = 0.45

Control System Variation
1sec. = 4.0sqs.

Figure 17

the system but has negligible effect upon the frequency of the root. The loss of amplitude is due to equipment troubles and has no significance.

The first step taken to improve the control was to study the effect of varying the derivative term in the feedback path. The oscillographs are collected in Figure 17, and the results in terms of frequency and damping are given in Figure 18.

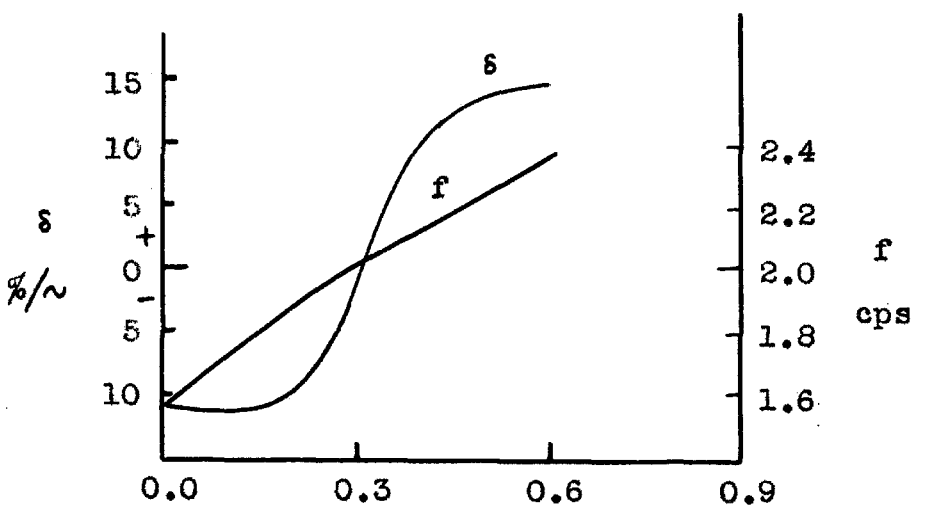

Effect of Varying r
$K_o H_o$ Control
Figure 18

Figure 19 presents the second part of the control modification, an examination of the effects of varying the delay times, $\tau 1$ and $\tau 2$. The oscillographs clearly indicate that reduction of

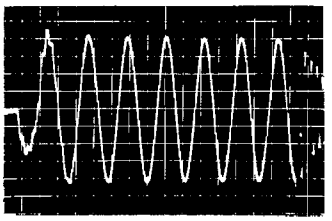

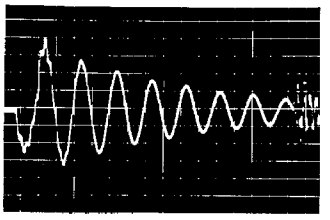

$\tau 2 = 0.05$

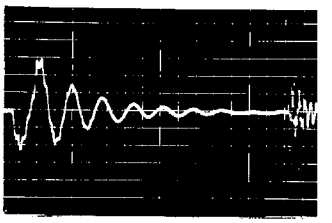

$\tau 1 = \tau 2 = 0.05$

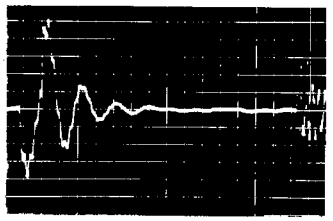

$\tau 2 = 0.0$

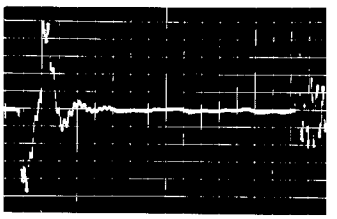

$\tau 1 = 0.05$
$\tau 2 = 0.0$

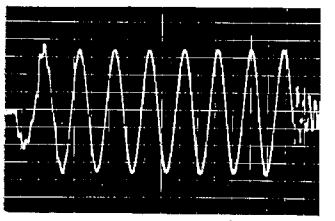

$\tau 2 = 0.05$ $K = 1.4$
$r = 0.2$

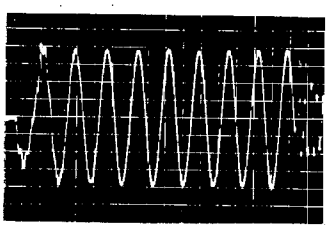

$\tau 2 = 0.05$ $K = 1.1$
$r = 0.45$

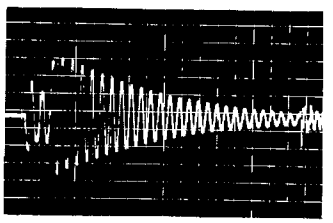

$\tau 2 = 0.0$ $K = 5.7$
$r = 0.6$

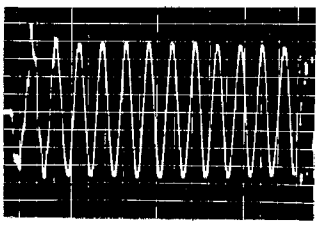

$\tau 1 = \tau 2 = 0.05$ $K = .75$
$r = 0.9$

Control System Variation
1sec. = 4.0sqs.

Figure 19

the delay times is a rapid way to achieve faster response with high gain. This is somewhat unrealistic because of the limited amount of standard apparatus which can meet such requirements. It was felt, however, that raising the system frequency would have significant effects, so a compromise control was chosen. The performance of the system with this K_1H_1 control is shown in the last oscillograph of Figure 19. The system frequency has been raised to 3.0cps. K_1 is also chosen for marginal stability to increase the sensitivity of the system to small parameter changes.

Figures 20 and 21 provide additional information on the relation between control system parameters and the overall system performance for more flexible fuselage structures. In Figure 20 the first five oscillographs show how the response changes from the K_oH_o reference condition case (first picture) as one of the delays is made zero, the gain increased, and the sensing device shifted aft along the missile. The lower half of the figure shows the same type of result when both the time delays are halved. Here again, variations in the delay times are a powerful means of altering the system response. With the more flexible 7.5cps fuselage beam, the high frequency root is of greater significance, particularly as the sensing point is moved toward the tail of the missile. In the last picture of

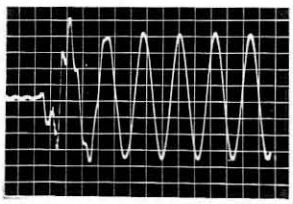

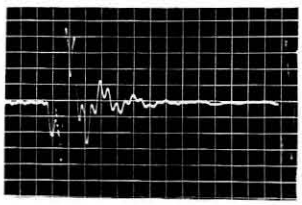

$\tau 2 = 0$

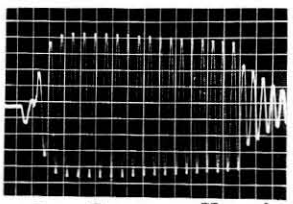

$\tau 2 = 0$ $K = 4.51$

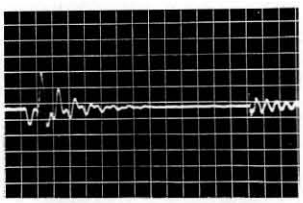

$\tau 2 = 0$ $K = 4.51$
SP75

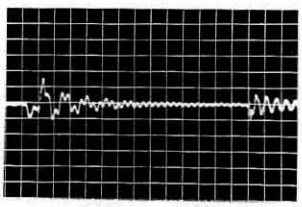

$\tau 2 = 0$ $K = 4.51$
SP125

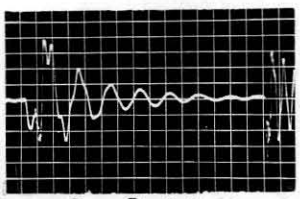

$\tau 1 = \tau 2 = 0.05$

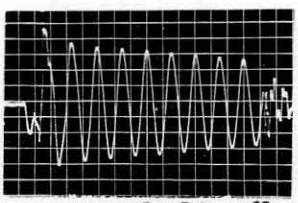

$\tau 1 = \tau 2 = 0.05$ $K = 1.6$

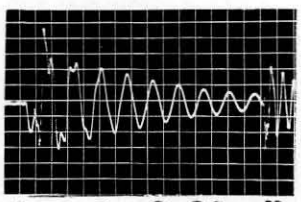

$\tau 1 = \tau 2 = 0.05$ $K = 1.6$
SP75

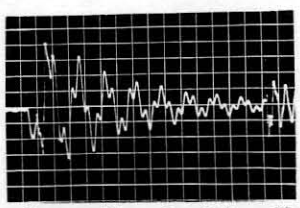

$\tau 1 = \tau 2 = 0.05$ $K = 1.6$
SP100

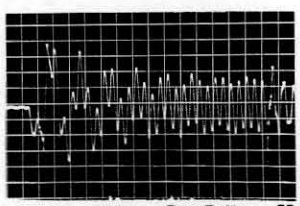

$\tau 1 = \tau 2 = 0.05$ $K = 1.6$
SP125

Control System Variations
1sec. = 4.2sqs. $f_1 = 7.5$cps

Figure 20

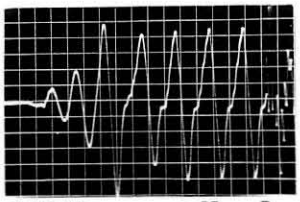
SP25 K = 1.51

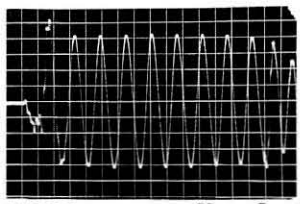
SP50 K = 1.51

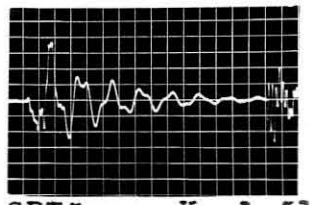
SP75 K = 1.51

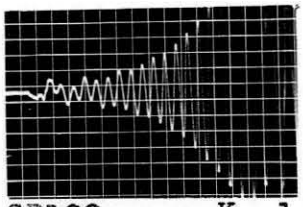
SP100 K = 1.51

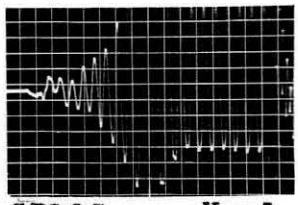
SP125 K = 1.51

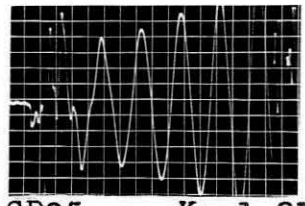
SP25 PP125 K = 1.01

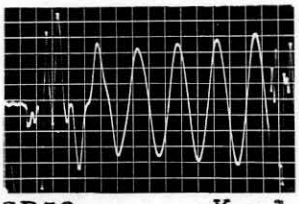
SP50 PP125 K = 1.01

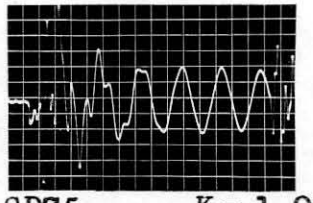
SP75 PP125 K = 1.01

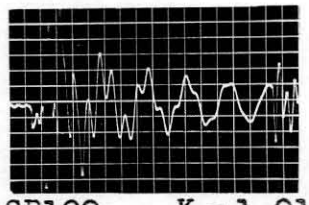
SP100 PP125 K = 1.01

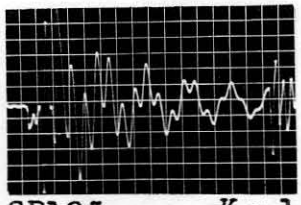
SP125 PP125 K = 1.01

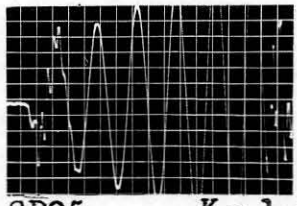
SP25 PP75 K = 1.01

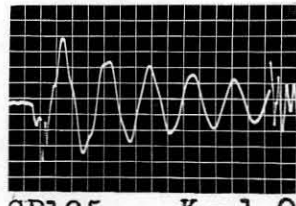
SP125 PP75 K = 1.01

Control System Variations
1sec. = 4.2sqs. $\tau 1 = \tau 2 = 0.05$ $f_1 = 4.7$cps

Figure 21

Figure 20 a situation is developing in which the low frequency root is well damped, but the high frequency root is almost unstable. This behavior is typical of the combination of a flexible fuselage and a sensing point aft of the center of the missile. It is caused by the difference in sign of the slopes of the first and second mode shapes on the after end of the fuselage. It would seem that the higher mode frequencies are low enough to influence the system in this fashion only for very flexible beams. Later results, however, will show that the condition is a relative one depending more nearly on the ratio of the fuselage f_1 to the controlled system frequency. Figure 21 is a similar case with a 4.7cps fuselage; with the sensing point moved aft to station 100, the low frequency root is almost completely damped out. The reader should take note that in some of the oscillographs showing unstable behavior only the first few cycles are of value due to overloading and distortion of the large signals.

C. A Controlled System With a Three Cycle Root.

As pointed out earlier the K_1H_1 control was devised to increase the system response frequency without going to unreasonably short delays. An increase of more than fifty percent from 2.0cps to 3.3cps was accomplished. This change has a large effect upon the system. Figure 22 is included only for completeness, presenting the slope angle

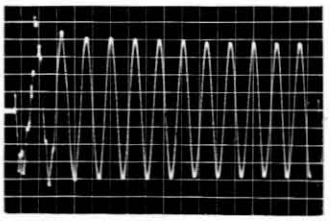

PP25 E_θ

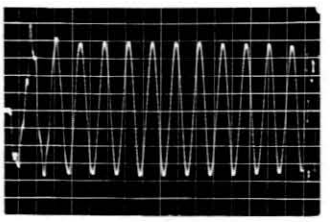

PP50 E_θ

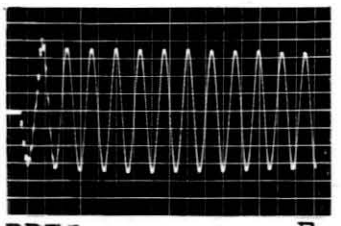

PP75 E_θ

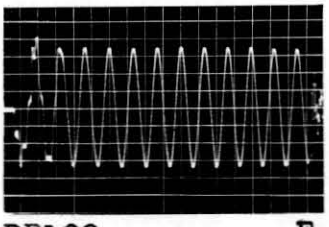

PP100 E_θ

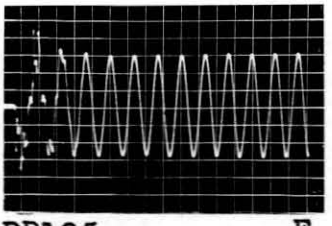

PP125 E_θ

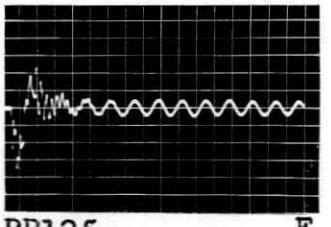

PP125 HFR E_θ

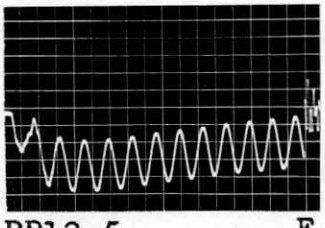

PP12.5 E_h

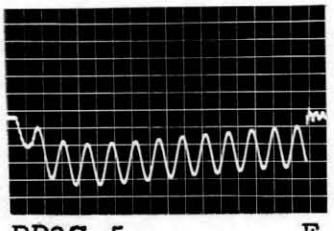

PP37.5 E_h

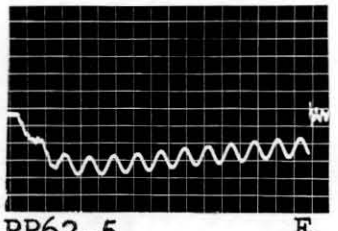

PP62.5 E_h

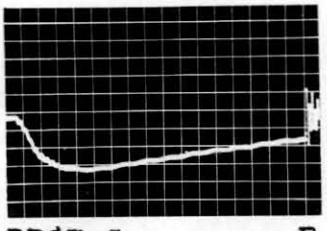

PP87.5 E_h

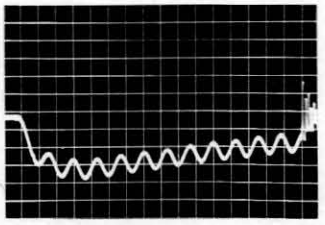

PP112.5 E_h

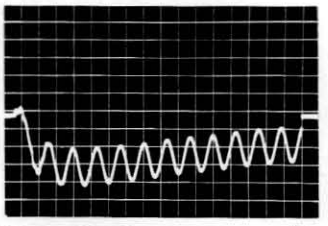

PP137.5 E_h

Complete Transient Behavior
1sec. = 4.3sqs. $f_1 = 15.0$cps K_1H_1 Control
Figure 22

response of the fuselage at five points and the vertical displacement behavior at six points. These pictures emphasize again the small size of the difference introduced by observing the missile response at different stations along the fuselage. This provides no information about moving the sensing point.

As was done for the K_oH_o system in Figures 11 through 14, the general change in performance with elasticity variations is shown in oscillographs in Figures 24 through 28. The damping increments and frequencies from this data are plotted in Figure 23.

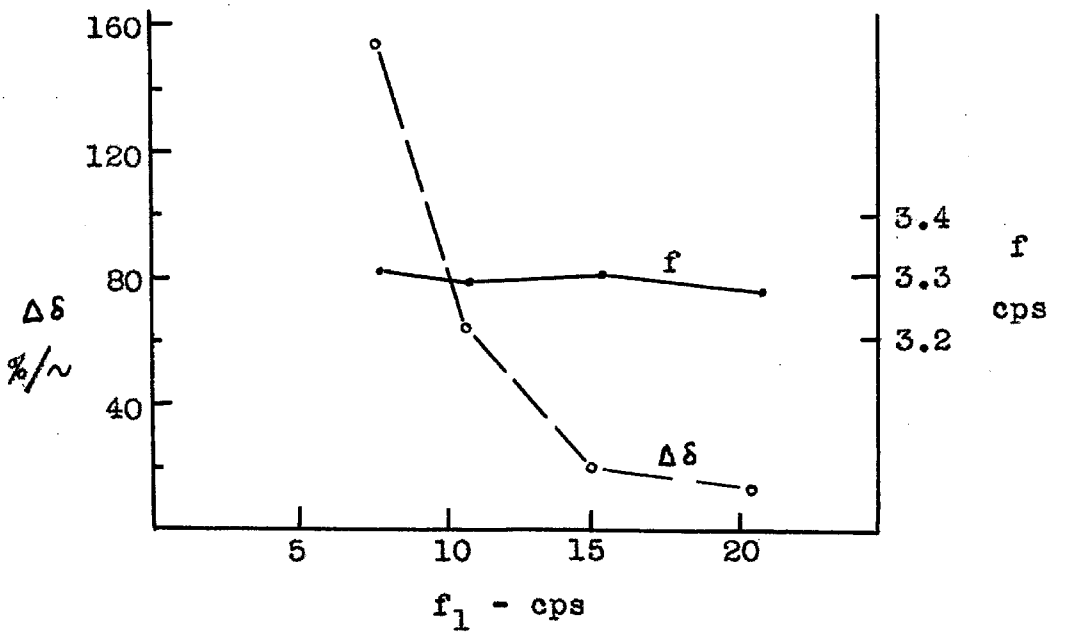

Effect of Varying Fuselage Elasticity
K_1H_1 Control
Figure 23

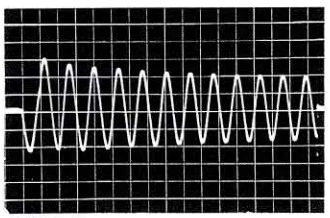

SP25

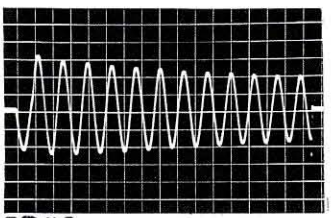

SP50

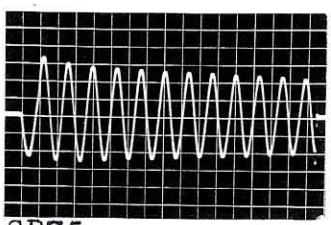

SP75

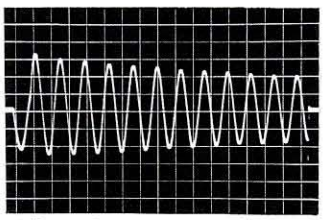

SP100

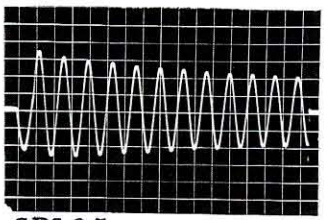

SP125

Variations in the Fuselage Structure
1sec. = 4.4sqs. $f_1 = \infty$ K_1H_1 Control
Figure 24

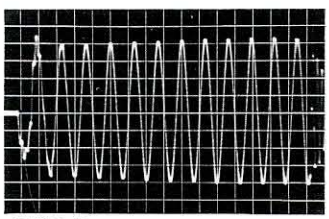

SP25

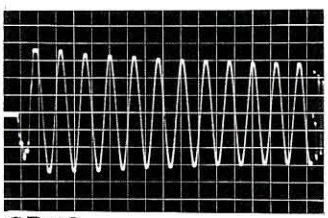

SP50

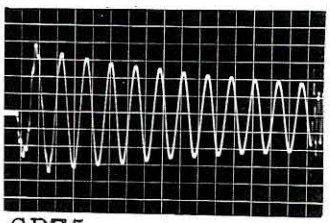

SP75

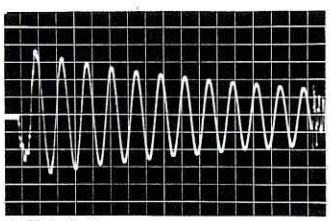

SP100

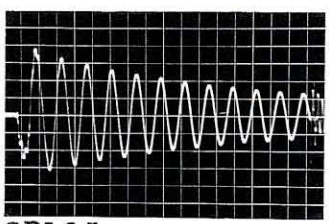

SP125

Variations in the Fuselage Structure
1sec. = 4.4sqs. $f_1 = 21.2$cps K_1H_1 Control
Figure 25

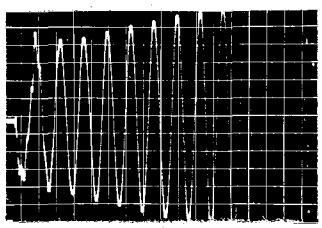

SP25

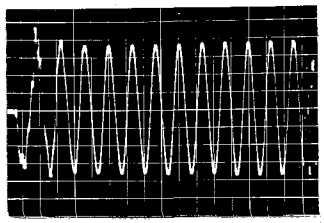

SP50

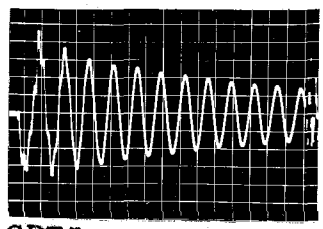

SP75

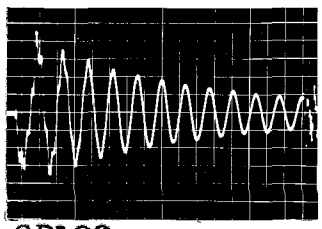

SP100

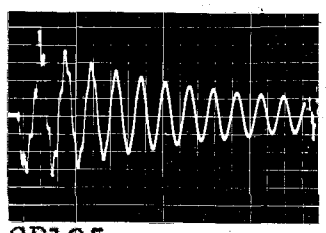

SP125

Variations in the Fuselage Structure
1sec. = 4.4sqs. f_1 = 15.0cps K_1H_1 Control
Figure 26

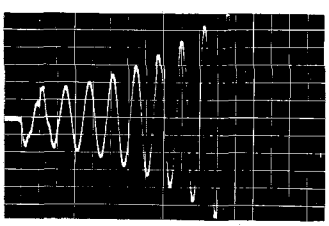

SP25

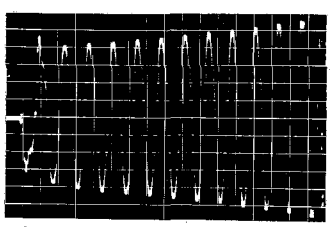

SP50

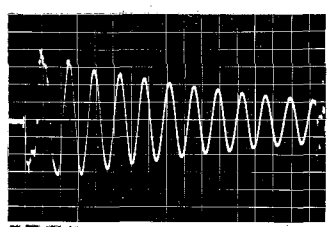

SP75

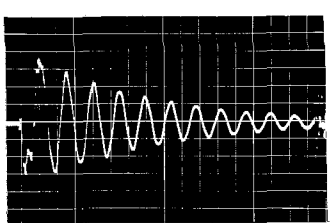

SP100

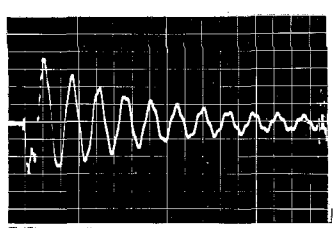

SP125

Variations in the Fuselage Structure
1sec. = 4.4sqs. f_1 = 10.6cps K_1H_1 Control
Figure 27

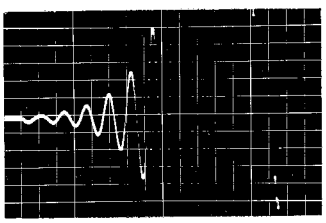

SP25

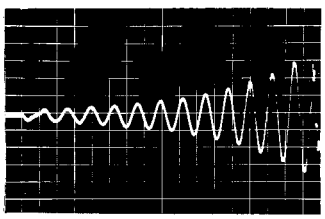

SP50

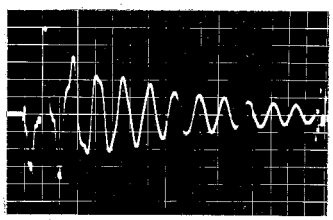

SP75

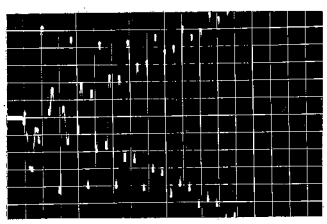

SP100

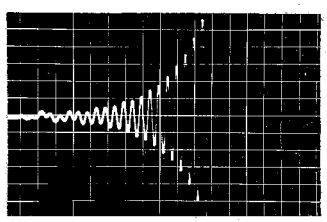

SP125

Variations in the Fuselage Structure
1sec. = 4.4sqs. $f_1 = 7.5$cps K_1H_1 Control
Figure 28

Comparing this with Figure 15, it is obvious that the stability of the K_1H_1 system is much more sensitive with respect to location of the sensing point than the K_oH_o system. The frequency is, however, almost independent of sensing device location. Examination of Figure 28 confirms the stability sensitivity, for the 7.5cps fuselage shows an unstable low frequency root with the sensing device forward and an unstable high frequency (9.2cps) root with the sensing device well aft. With the K_oH_o system such behavior was only found with the most flexible fuselage beams. Even in the case shown in Figure 20, where the frequency had been increased to 2.7cps by reducing the delays, the 7.5cps fuselage was only beginning to show signs of this double root behavior. Two combinations of parameters have resulted in an increased system response frequency. The first, the results of which are shown in Figure 20, is a combination of moderate delays and a moderate rate coefficient. The second, used in the K_1H_1 control, combines moderate-to-small delays with a large rate term. In Section VI-D a third combination of low delays and low rate term will be used to further increase the response frequency. The effect of such increases seems to be an increased sensitivity to parameter variations in general and to fuselage elasticity effects in particular. The nature of these changes appears to be independent of the method used to raise the frequency, and the extent of the changes is determined by the amount of frequency increase.

Since an actual missile is not uniform in structure over its length it is important to see how this will change the system response. Figure 29 is the behavior of a fuselage beam which has a tapered structure. The value of EI at the tail is zero; at the nose it has twice the value corresponding to the uniform reference condition 15.0cps beam. The average value of EI over the tapered beam is then equal to the reference value of EI. Figure 30 presents the performance of a similar fuselage with the taper reversed, so that the tail is stiff and the nose flexible. Comparing both of these with the K_1H_1, 15.0cps case, Figure 26, it is seen that the behavior is essentially unaffected as long as the sensing point remains at station 50. There is a slight increase in damping but the frequency is unchanged. When the sensing point is shifted, the resulting effect is exaggerated if the shift is toward the flexible end of the fuselage and subdued if the shift is toward the stiff end. It would seem that a fuselage without extraordinary stiffness irregularities could be adequately represented by a uniform beam having the same average stiffness.

The remaining oscillographs included in Section VI-C are devoted to a brief investigation of the effects of variations in some of the aerodynamic parameters. Figures 31 through 34 show how the missile's behavior and sensitivity to sensing point location change over a range of speeds and

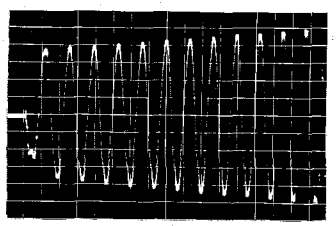

SP25

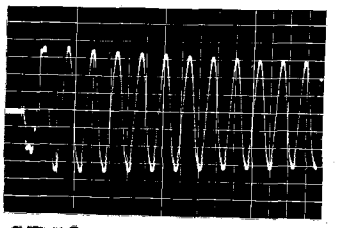

SP50

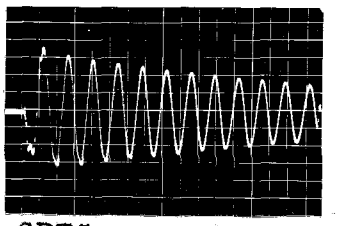

SP75

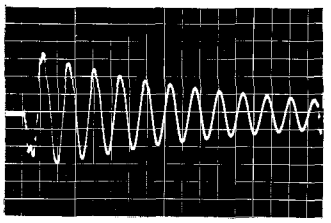

SP100

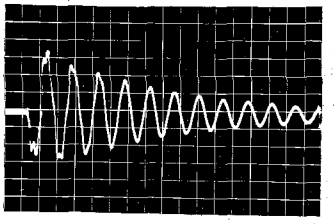

SP125

Variations in the Fuselage Structure
1sec. = 4.3sqs. Tapered Beam, Stiff Nose K_1H_1 Control

Figure 29

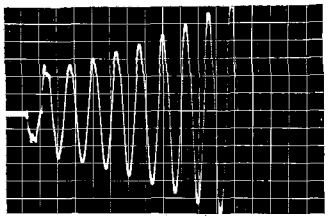

SP25

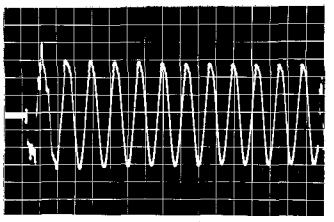

SP50

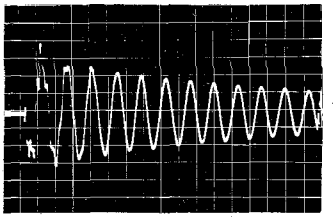

SP75

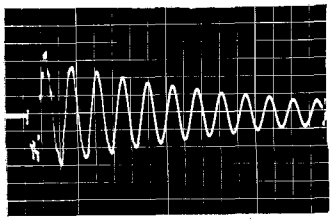

SP100

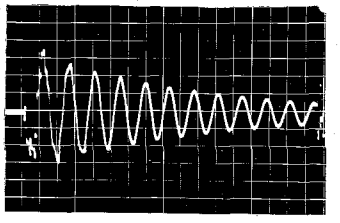

SP125

Variations in the Fuselage Structure
1sec. = 4.3sqs. Tapered Beam, Stiff Tail K_1H_1 Control

Figure 30

altitudes from Mach 1.0 at 15,000 feet to Mach 2.0 at 60,000 feet. Increased speed without change of altitude or loss of altitude both tend to destabilize the system by increasing the aerodynamic forces and, thus, effectively increasing the system gain. A maximum of 12 db gain reduction was required to restore stability in the case in which the flight velocity was doubled. Less than 6 db reduction was required to compensate for halving the flight altitude. Since the study system was deliberately made marginally stable to begin with, these figures do not apply directly to a practical control, but they do provide an indication of the kind of gain margin required for operation over such a range of conditions. Increased speed raises the system frequency slightly, and an increase in altitude seems to slightly subdue the high frequency root. The general nature of the system is unchanged by changes of altitude and speed, and it is expected that the same effects of fuselage elasticity which were observed on more flexible beams at fixed altitude and speed will be found to act over the entire range of operation of the missile.

Figure 35 shows the variation in system response as the downwash ratio, k, is varied from 0.0 to 0.32. As k is increased, the tendency is toward destabilization, because downwash reduces the aerodynamic effectiveness of the tail surface. By comparison with Figure 16 it is seen

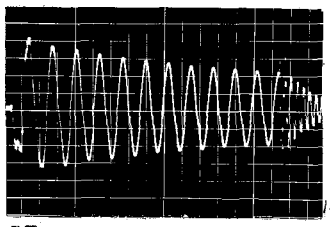

SP25

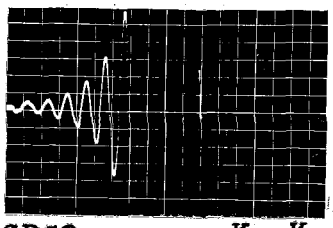

SP50 $K = K_1$

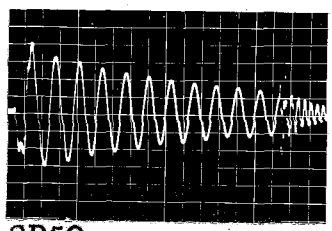

SP50

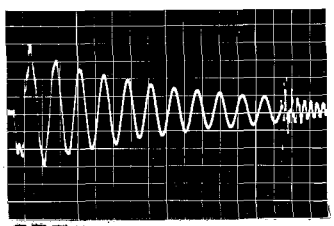

SP75

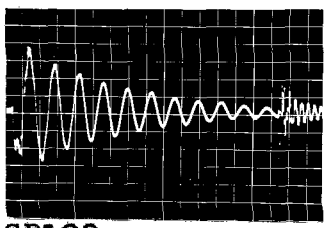

SP100

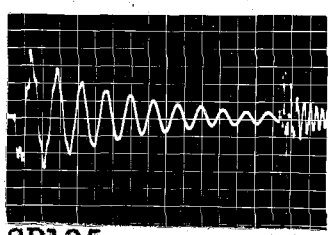

SP125

Varying Altitude and Speed
Mach 1.0 at 15,000ft. $f_1 = 15$cps $K = 0.37$ H_1 Control
1sec. = 4.2sqs.

Figure 31

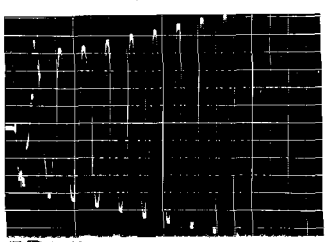

SP25

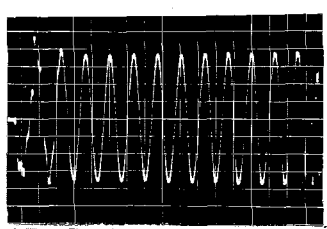

SP50

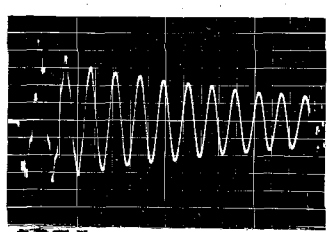

SP75

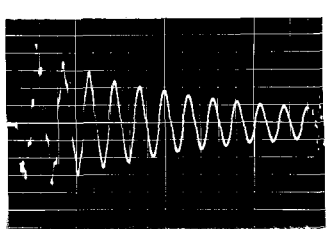

SP100

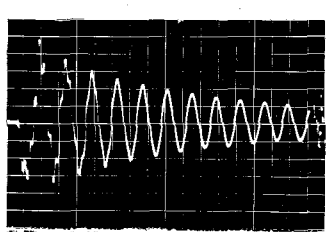

SP125

Varying Altitude and Speed
Mach 1.0 at 30,000ft. $f_1 = 15$cps $K_1 H_1$ Control
1sec. = 4.4sqs.

Figure 32

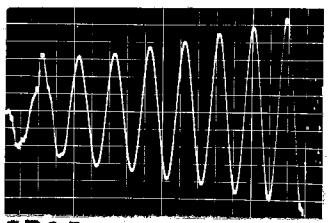
SP25

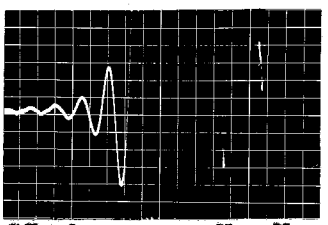
SP50 K = K_1

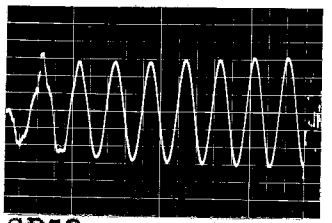
SP50

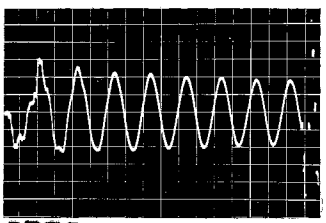
SP75

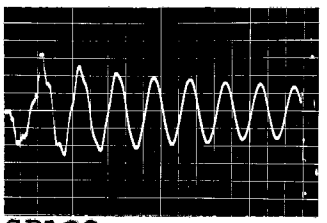
SP100

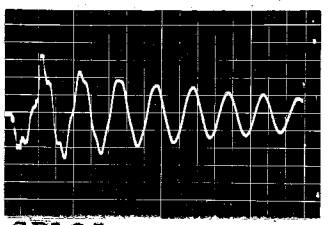
SP125

Varying Altitude and Speed
Mach 2 at 30,000ft. f_1 = 15cps K = 0.2 H_1 Control
1sec. = 8.0sqs.

Figure 33

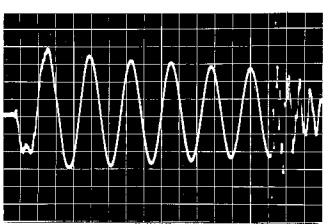
SP25

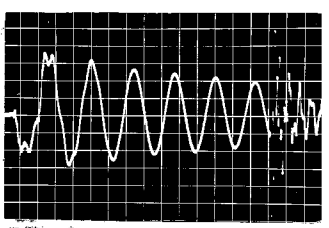
SP50

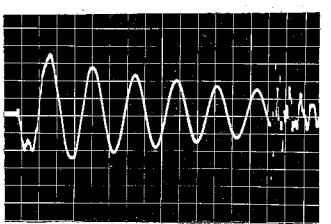
SP75

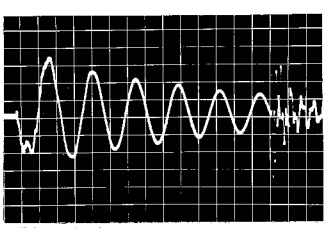
SP100

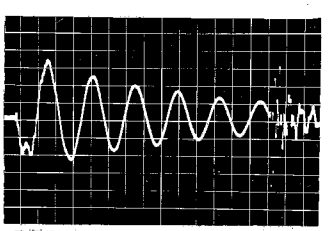
SP125

Varying Altitude and Speed
Mach 2 at 60,000ft. f_1 = 15cps K_1H_1 Control
1sec. = 7.7sqs.

Figure 34

that raising the controlled frequency has increased the sensitivity of the system to changes in k as well as to elasticity effects.

Figures 36 and 37 demonstrate the results of changing the areas of the airfoils. The effect on the two surfaces is the same; an increased area on either appears as an increase in system gain, decreasing the damping and raising the frequency. The control surface area change produces a greater effect, since it is directly in series with the control system.

Figures 38 and 39 are two sets of oscillographs illustrating the change in the system root caused by changes in the position of the two airfoils. When one or both of the surfaces were moved, the downwash delay time had to be adjusted accordingly. The frequency reducing effect of moving the tail surface was anticipated, but elastic deformation of the fuselage is also contributing to the observed result. In shifting the airfoils, particularly the forward surface, the elastic variations in behavior along the beam are being introduced into the system just as though the feedback sensing point were being moved. The reader will note that the effect of moving the control surface is exactly the same as that of moving the sensing device including negative damping forward, increased positive damping aft, and the appearance of the high frequency root as the control is moved aft.

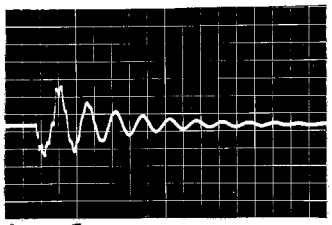

k = 0

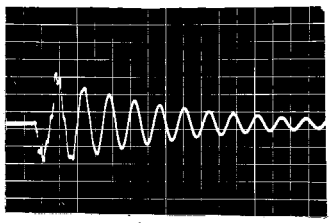

k = 0.08

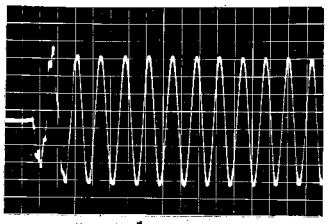

k = 0.16

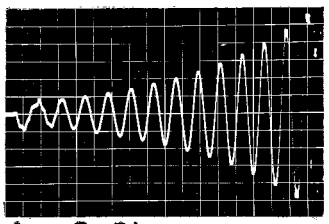

k = 0.24

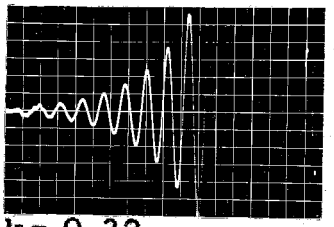

k = 0.32

Changing Downwash Ratio
1sec. = 4.3sqs. f_1 = 15cps K_1H_1 Control
Figure 35

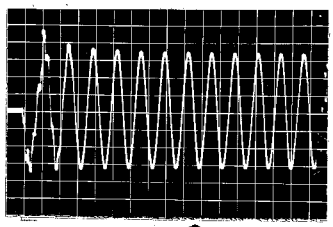

$S_1 = 200in^2$

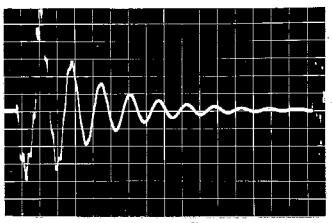

$S_1 = 100in^2$

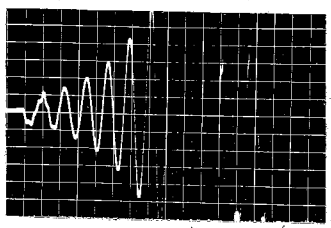

$S_1 = 300in^2$

Changing Control Surface Area
1sec. = 4.2sqs. $f_1 = 15cps$ K_1H_1 Control
Figure 36

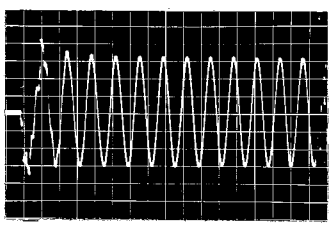

$S_2 = 375in^2$

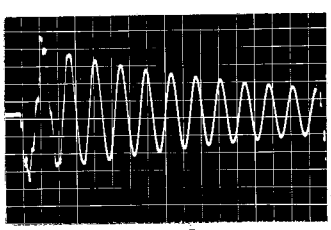

$S_2 = 250in^2$

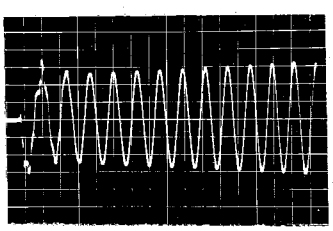

$S_2 = 500in^2$

Changing Tail Surface Area
1sec. = 4.2sqs. $f_1 = 15cps$ K_1H_1 Control
Figure 37

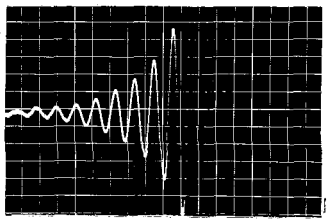

$X_1 = 12.5$

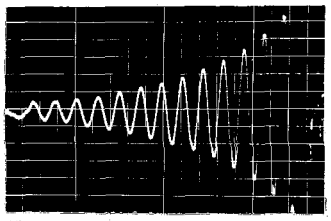

$X_1 = 37.5$

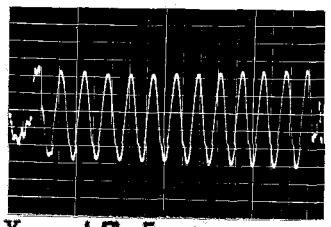

$X_1 = 47.5$

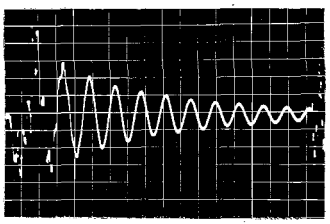

$X_1 = 62.5$

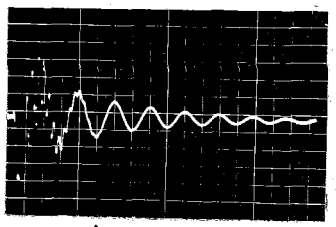

$X_1 = 87.5$

Changing the Location of the Control Surface
1sec. = 4.0sqs. $f_1 = 15$cps K_1H_1 Control
Figure 38

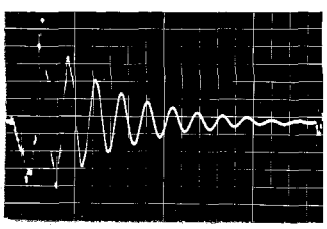

$X_2 = 107.5$

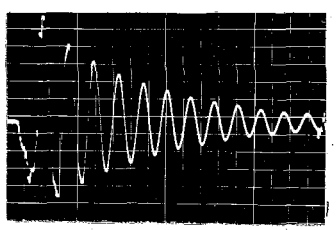

$X_2 = 117.5$

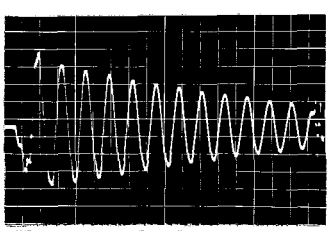

$X_2 = 127.5$

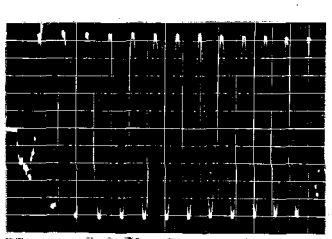

$X_2 = 137.5$

Changing the Location of the Tail Surface
1sec. = 4.0sqs. $f_1 = 15$cps K_1H_1 Control
Figure 39

D. A Controlled System With a Higher Response Frequency.

Though the K_1H_1 control system avoided extremely short delays, it was unrealistic in that an unusually large rate coefficient, r, was used to raise the controlled frequency. It may be more appropriate to choose a system which is a designer's goal in the sense that it represents a presently unattainable, but hoped for, device. Furthermore, the data already presented has clearly demonstrated that high system frequency and low fuselage frequency are the combination required to obtain more interesting and significant results. Thus, a third control system, K_2H_2, with a low rate term and extremely low delay times, is devised. K_2 is the value of gain required to produce marginal stability, so that the system will show maximum sensitivity to disurbing effects. The K_2H_2 control raises the system frequency to 6.2cps. Figure 40 is the complete record of the behavior of the 15.0cps reference fuselage combined with the K_2H_2 control. Its motion appears to be centered about a point aft of the center of the missile with the nose undergoing relatively large amplitude oscillations compared to the tail. It is apparent at this stage that raising the system frequency to 6.2cps has altered the behavior very considerably; previous systems showed no such phenomenon as observed in Figure 40.

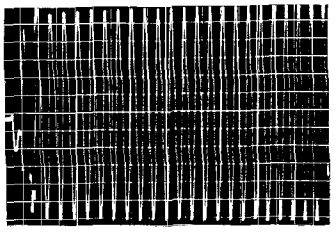

PP25

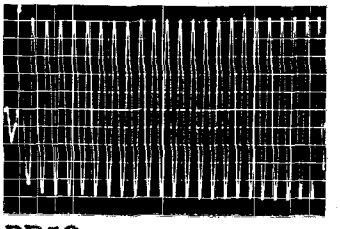

PP50

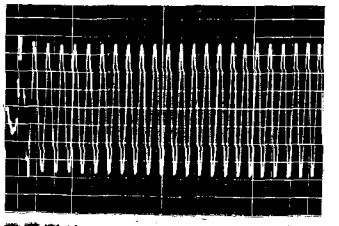

PP75

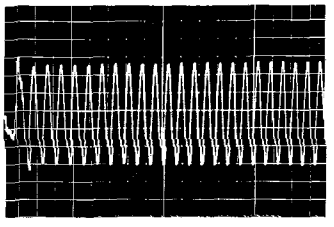

PP100

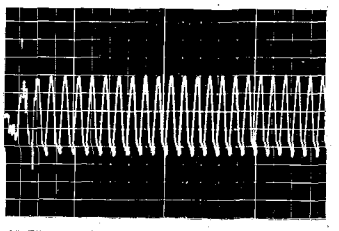

PP125

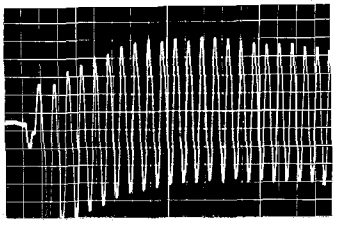

PP12.5

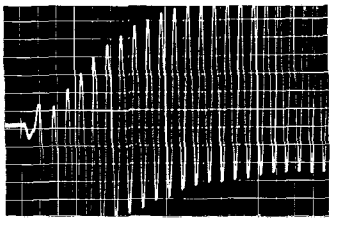

PP37.5

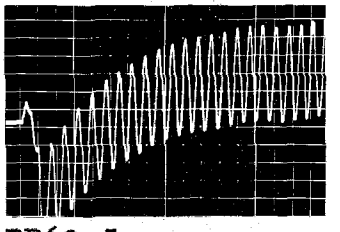

PP62.5

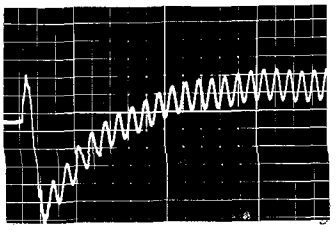

PP87.5

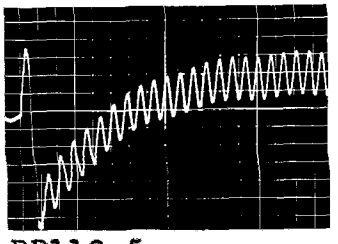

PP112.5

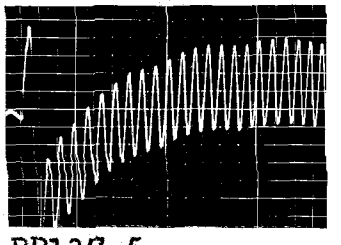

PP137.5

Complete Behavior of Improved System
1sec. = 4.6sqs. f_1 = 15.0cps K_2H_2 Control
Figure 40

An investigation of the effects of moving the sensing point and varying the fuselage flexibility similar to that performed on each of the previous systems was carried out on this system. Figures 41 through 45 display the resulting oscillographs. It is difficult to graphically present the behavior of this system by itself, or as a comparison with the other systems, because there are now two different important roots. With measurements only available at a discrete number of points it is impossible to determine at exactly what sensing point a particular root becomes lost or to obtain a worthwhile plot of root behavior against sensing point location. The author's purpose in presenting the earlier plots was largely to offer numerical evidence that the alleged trends existed when they were not yet obvious.

The K_2H_2 system is particularly interesting because it is extremely critical. There is a large stabilizing effect produced when the rigid beam is introduced in place of the 15.0cps beam. Some such reaction is to be expected since a rigid beam <u>is</u> less flexible than a 15.0cps beam; however, the same difference in beam structures failed to produce anything like this effect with the first control systems. The unusual double root effect has appeared fully in the 21.2cps beam case which heretofore was hard to distinguish from the rigid case. As was the case for the

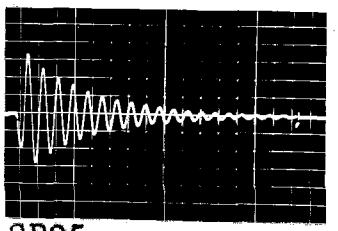
SP25

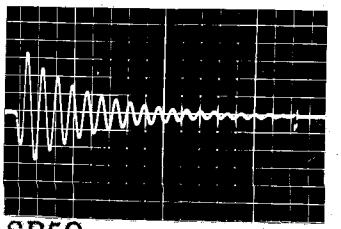
SP50

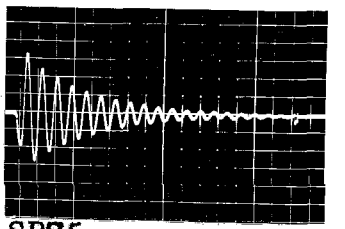
SP75

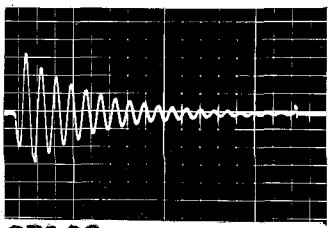
SP100

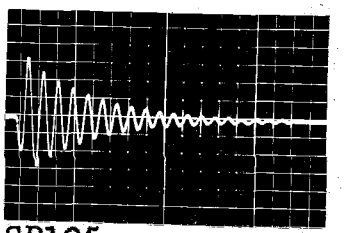
SP125

Variations in Fuselage Structure
lsec. = 4.6sqs. $f_1 = \infty$ K_2H_2 Control
Figure 41

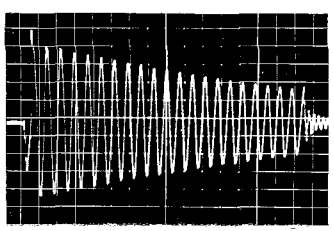
SP25

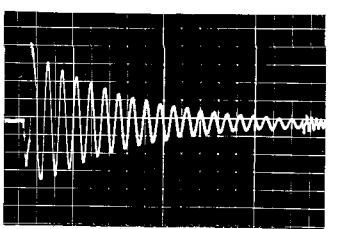
SP50

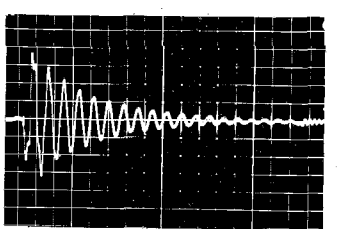
SP75

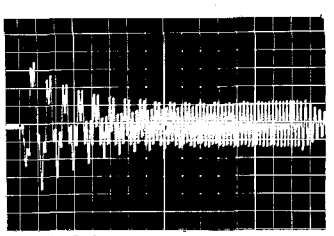
SP100

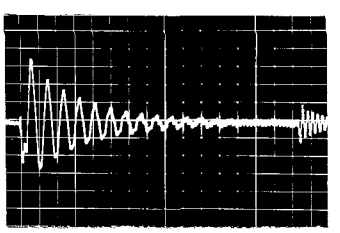
SP100 LFR

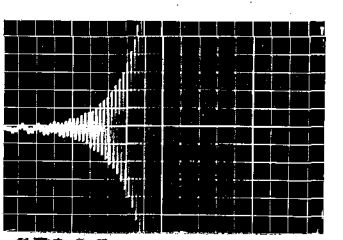
SP125

Variations in Fuselage Structure
lsec. = 4.6sqs. $f_1 = 21.2$cps K_2H_2 Control
Figure 42

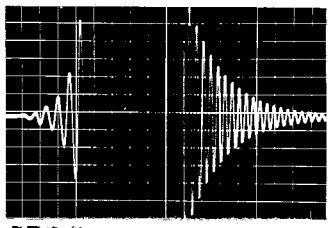
SP25

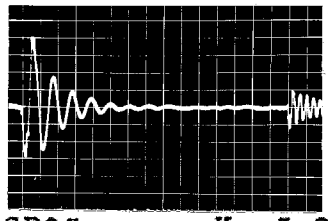
SP25 K = 5.2

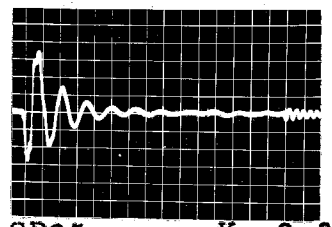
SP25 K = 3.3

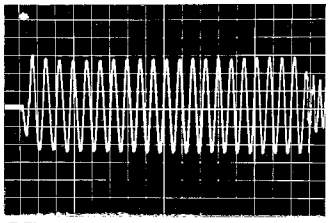
SP50

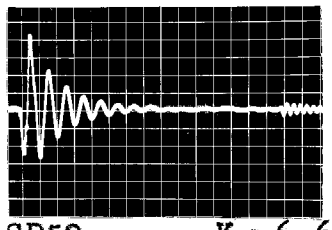
SP50 K = 6.6

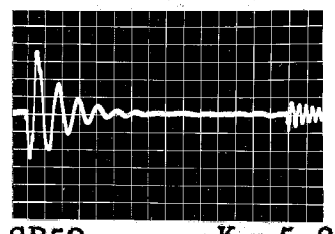
SP50 K = 5.2

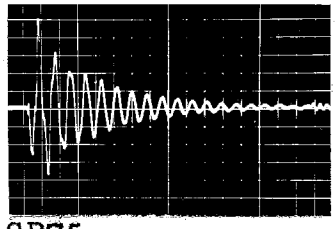
SP75

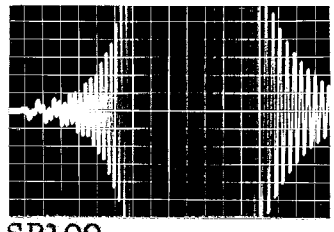
SP100

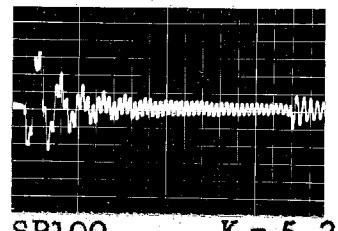
SP100 K = 5.2

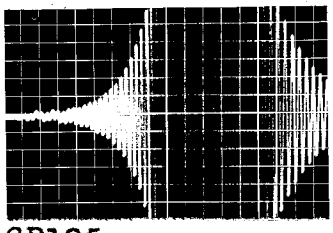
SP125

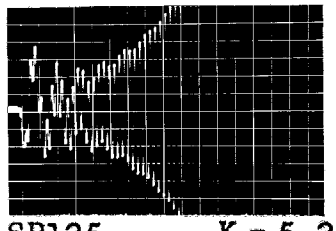
SP125 K = 5.2

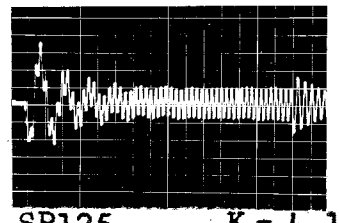
SP125 K = 4.1

Variations in Fuselage Structure
1sec. = 4.6sqs. f_1 = 15.0cps K_2H_2 Control

Figure 43

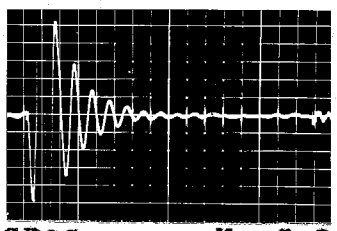

SP25 K = 5.2

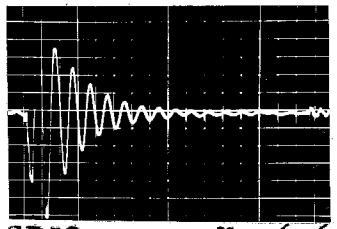

SP50 K = 6.6

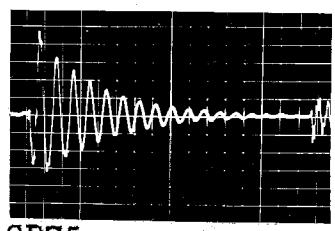

SP75

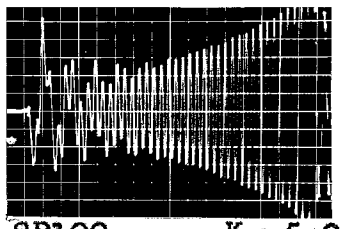

SP100 K = 5.2

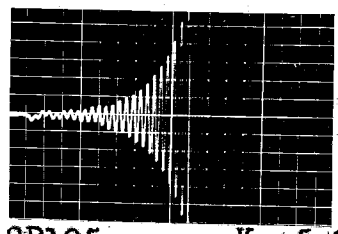

SP125 K = 5.2

Variations in Fuselage Structure
1sec. = 4.6sqs. f_1 = 10.6cps K_2H_2 Control
Figure 44

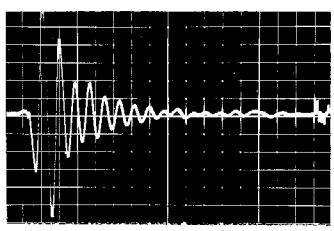

SP25 K = 3.3

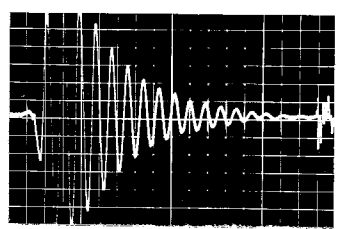

SP50 K = 5.2

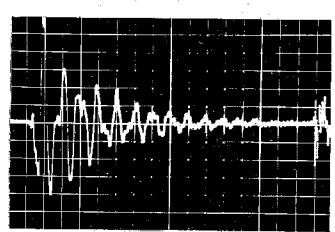

SP75

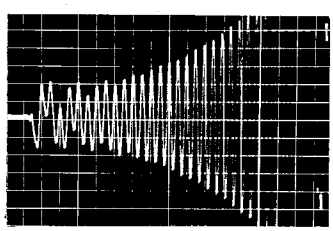

SP100 K = 5.2

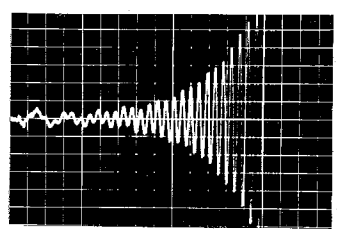

SP125 K = 4.1

Variations in Fuselage Structure
1sec. = 4.6sqs. f_1 = 7.5cps K_2H_2 Control
Figure 45

more flexible beams, the high frequency root (23cps for the 21.2cps beam) is excited and the low frequency root (5.2cps) subdued due to the sign difference between the first and second fuselage mode shape slopes in the after part of the missile.

The response of the 15.0cps fuselage combined with the K_2H_2 control is pictured in Figure 43. With the full gain, $K_2 = 10.4$, the system goes unstable when the sensing point is moved one station forward (low frequency root) or two stations aft of the normal station 50 location. The large number of additional oscillographs with different values of K are provided for comparison with the 10.6cps and 7.5cps cases which were so unstable with full gain that their behavior was recorded with reduced values of K. The 10.6cps and 7.5cps cases in Figures 44 and 45 are of a similar nature, but the effects are even more obvious.

It is possible to compare by inspection the apparent damping increment between SP25 and SP125 for the 7.5cps beam with that for the 15.0cps beam or the 21.2cps beam, and, remembering that the 7.5cps case was recorded with reduced gain, it is obvious that the sensitivity of the system to sensing point location increases rapidly as the fuselage frequency decreases. This lends additional support to the idea that the important parameter in discussing the effects of fuselage elasticity is the ratio of the fuselage

first bending mode frequency to the controlled natural frequency of the system.

Figure 46 demonstrates that the increased sensitivity to elasticity effects is accompanied by equally sensitive response to variations in other parameters. The six pictures across the top of the figure show a radical change in system behavior going from unstable at the high frequency root to unstable at the low frequency root as the rate coefficient, r, is reduced from 0.0675 to 0.038. The location of the sensing point at station 100, of course, is part of the explanation of this behavior. The four photographs at the bottom of Figure 46 are representative of a large number of conditions which were examined while looking for further improvement in control performance. Each one represents the optimum value of r, assuming the other parameters to be fixed as indicated.

E. The System of Section VI-D Readjusted to Provide an 8 db Gain Margin.

All of the measurements previously presented were made with the system adjusted for marginal stability in order to more easily detect the results of parameter variations. To bring the results of this work a little closer to practicality a final series of measurements were made with a control system having 8 db of gain margin. This system, called the K_3H_2 control, is identical to that discussed in

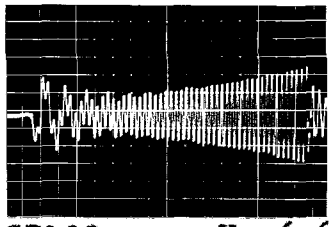

SP100 K = 6.6

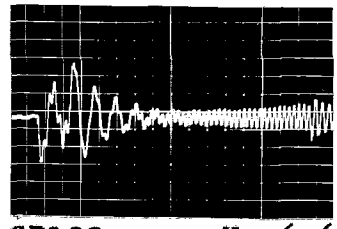

SP100 K = 6.6
LFR

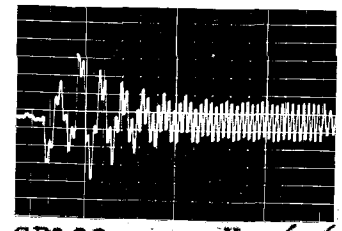

SP100 K = 6.6
r = 0.060

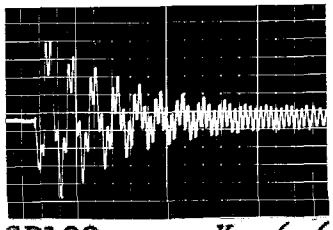

SP100 K = 6.6
r = 0.052

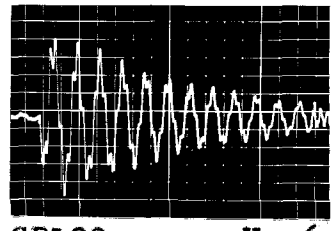

SP100 K = 6.6
r = 0.045

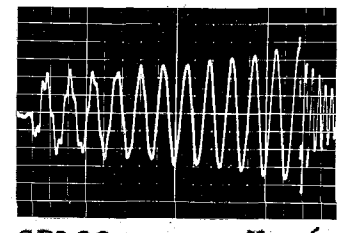

SP100 K = 6.6
r = 0.038

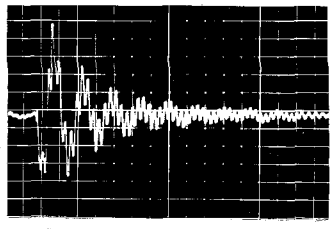

SP125 K = 3.3
r = 0.066

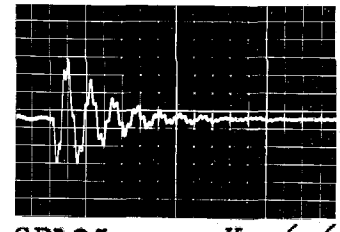

SP125 K = 6.6
r = 0.050 τ2 = 0.0

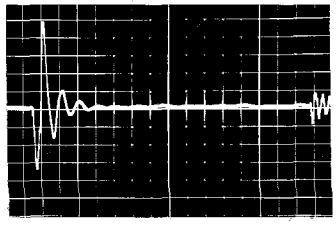

SP25 K = 4.1
r = 0.105

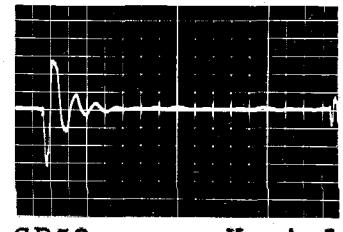

SP50 K = 4.1
r = 0.100

Control System Variations
1sec. = 4.5sqs. f_1 = 15.0cps K_2H_2 Control
Figure 46

Section VI-D except for the substitution of $K_3 = 4.1$ for $K_2 = 10.4$.

The 8 db figure was chosen to give a 4.0cps damped root with the 15.0cps fuselage. Figure 47 shows concisely how this particular control reacts with fuselages of varying stiffness. With K reduced by 8 db there is not much difference between the response of a 15.0cps fuselage and that of a rigid one, but a hint of the 15.0cps beam's higher modes shows in the first cycle of the top right picture. With a 7.5cps fuselage the response begins to show signs of increasing frequency; then, as f_1 is further decreased, the system behavior changes rapidly until it is just about to become unstable at 5.0cps when the fuselage first bending mode frequency has been reduced to 6.25cps.

The effects of moving the sensing point are still significant even though the system now has some stability reserve. Figures 48 through 51 show that choosing the proper location of the sensing point is important although the effects are no longer so severe. In Figures 48 and 49 the increased sensitivity acquired in halving the fuselage frequency is very evident. In the $f_1 = 15.0$cps case the sensing point could be located anywhere from station 25 to about station 85 without seriously affecting the response. If the fuselage is more flexible, with $f_1 = 7.5$cps, the sensing point must be between stations 50 and 75 for good

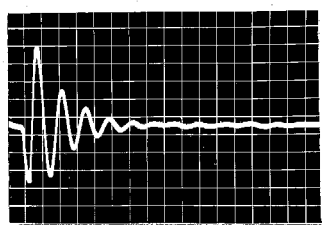

$f_1 = \infty$

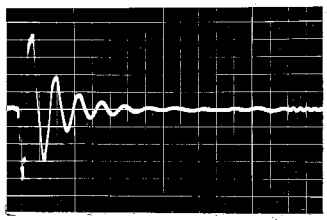

$f_1 = 15.0$

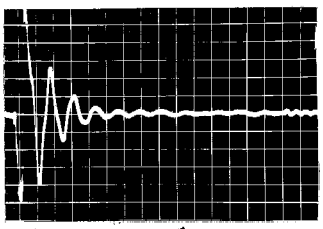

$f_1 = 10.6$

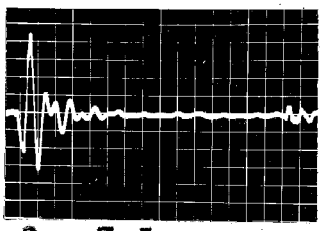

$f_1 = 7.5$

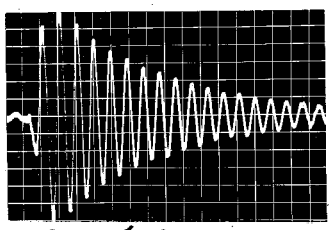

$f_1 = 6.4$

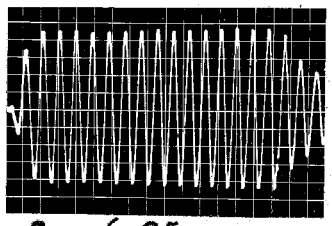

$f_1 = 6.25$

Fuselage Structure Variations
1sec. = 4.7sqs. K_3H_2 Control
Figure 47

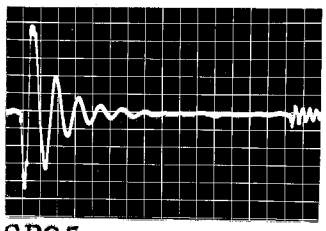

SP25

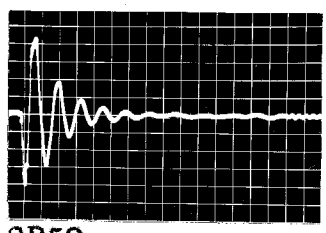

SP50

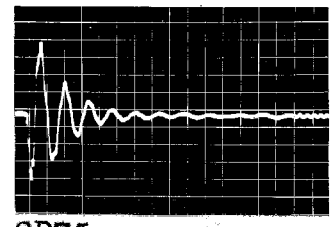

SP75

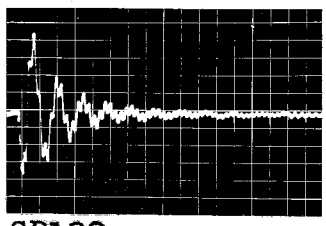

SP100

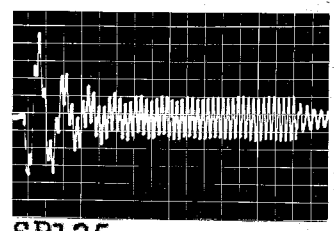

SP125

Fuselage Structure Variations
lsec.= 4.7sqs. f_1 = 15.0cps K_3H_2 Control
Figure 48

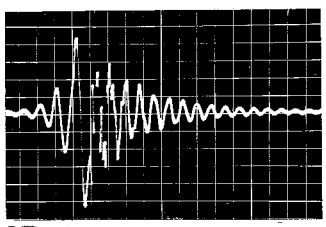

SP25

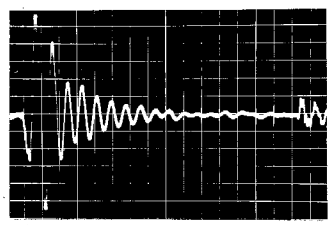

SP25 K = 3.3

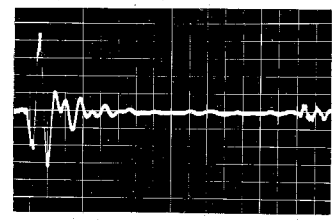

SP50

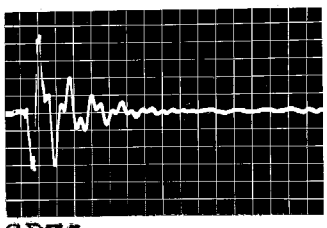

SP75

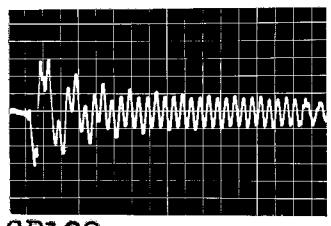

SP100

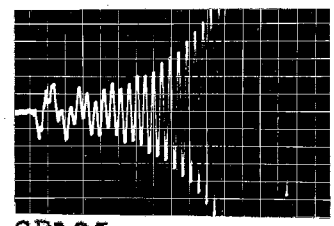

SP125

Fuselage Structure Variations
lsec.= 4.7sqs. f_1 = 7.5cps K_3H_2 Control
Figure 49

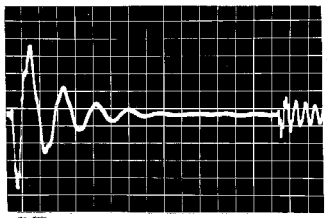

SP25

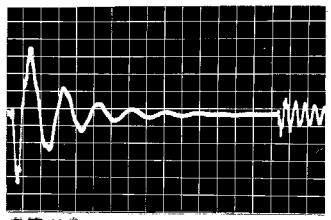

SP50

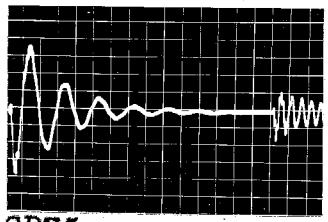

SP75

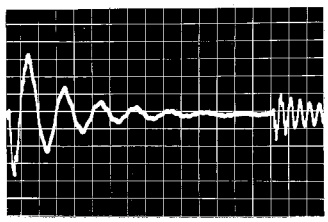

SP100

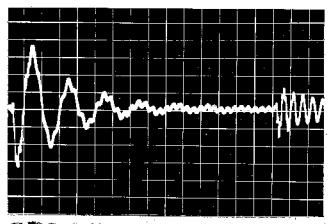

SP125

Fuselage Structure Variations
W = 1500lbs. f_1 = 10.6cps
1sec. = 4.6sqs. K_3H_2 Control

Figure 50

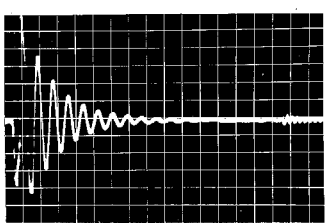

SP25

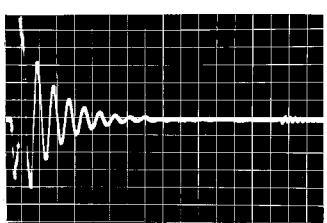

SP50

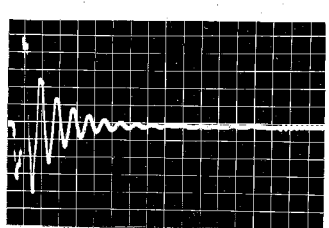

SP75

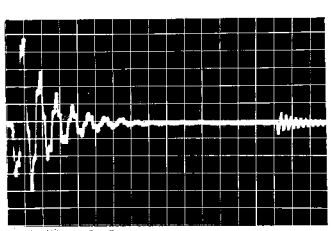

SP100

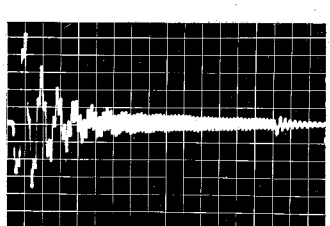

SP125

Fuselage Structure Variations
W = 375lbs. f_1 = 21.2cps
1sec. = 4.6sqs. K_3H_2 Control

Figure 51

performance. In both cases it is easily possible to develop instability of the high frequency root if the sensing device is located appreciably aft of station 75.

Figures 50 and 51 show how the system is affected by changes in the weight of the missile. The EI product is not changed from the $f_1 = 15.0$cps reference case. The effect of changing the mass is largely to alter the frequency; in the simple system of VI-A it varies inversely as the square root of the weight. That result is clearly shown in the oscillographs. Both systems, like all of the preceding ones, show the tendency to break into higher frequency oscillations if the sensing device is placed too far aft.

It was mentioned in Part II that the present practice of aeronautical engineers is to minimize the downwash effect by adjusting the ratio of the spans. Because of this practice, the K_3H_2 system was exposed to some aerodynamic parameter variations both with and without downwash. Figure 52 shows the effect of eliminating downwash with three different fuselage structures. The high frequency root is encouraged somewhat, but there are no major effects. Figure 53 presents the effect of moving the tail surface, with and without downwash. Again, there are no important changes observed. As in Figure 52, however, the elimination of the downwash seems to encourage the high frequency root. Finally, Figures 54 and 55 show how moving

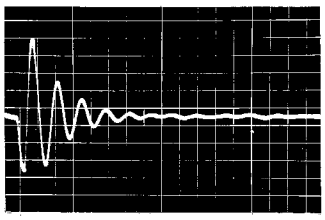

$f_1 = \infty$

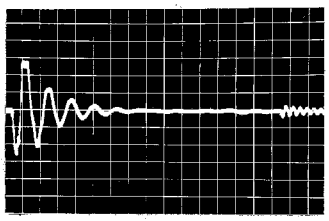

$f_1 = 15.0$

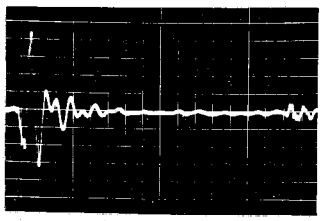

$f_1 = 7.5$

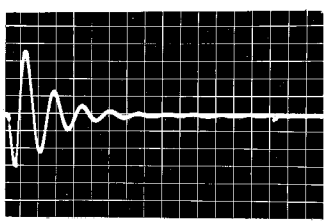

$f_1 = \infty$ k = 0

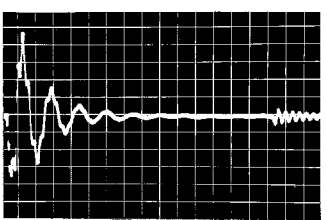

$f_1 = 15.0$ k = 0

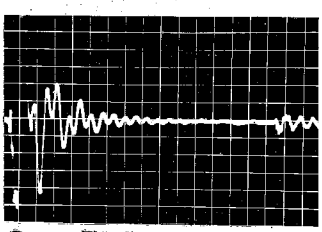

$f_1 = 7.5$ k = 0

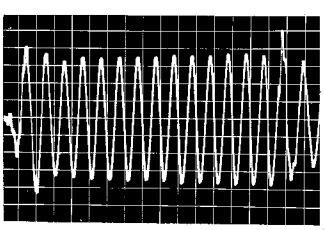

$f_1 = 4.7$ k = 0

Changing the Downwash Ratio
lsec. 4.6sqs. K_3H_2 Control
Figure 52

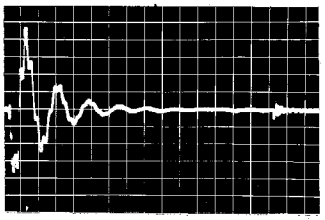

$X_2 = 107.5$ k = 0

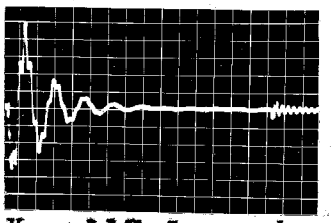

$X_2 = 117.5$ k = 0

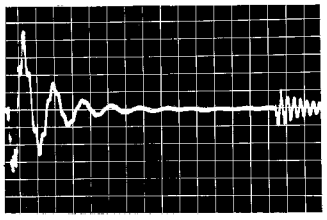

$X_2 = 127.5$ k = 0

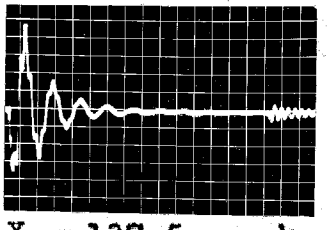

$X_2 = 137.5$ k = 0

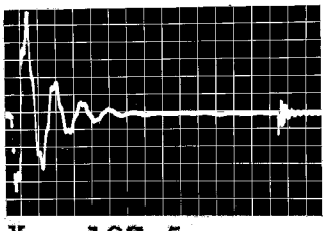

$X_2 = 107.5$

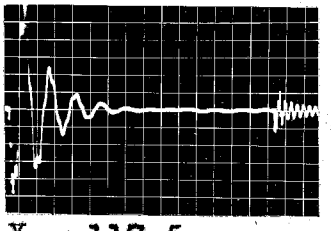

$X_2 = 117.5$

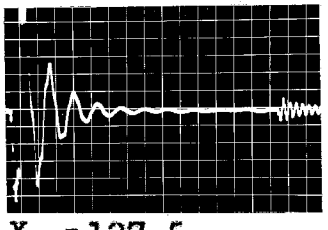

$X_2 = 127.5$

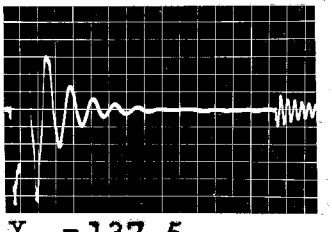

$X_2 = 137.5$

Shifting Tail Surface Location
1sec. = 4.6sqs. $f_1 = 15.0$cps K_3H_2 Control
Figure 53

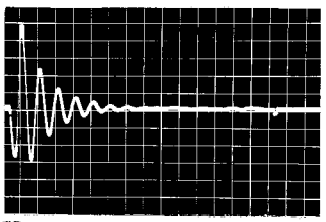

$X_1 = 12.5 \quad f_1 = \infty$

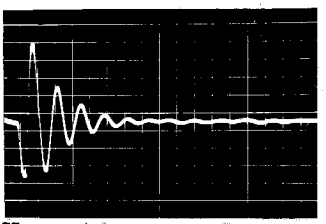

$X_1 = 47.5 \quad f_1 = \infty$

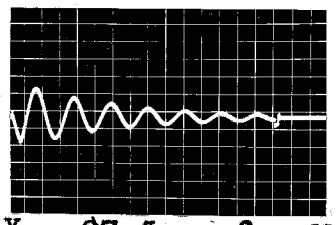

$X_1 = 87.5 \quad f_1 = \infty$

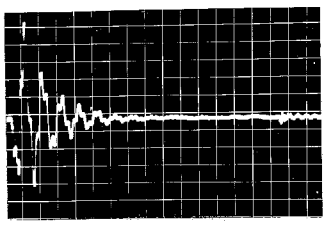

$X_1 = 12.5 \quad f_1 = 15$

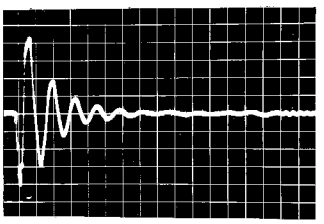

$X_1 = 47.5 \quad f_1 = 15$

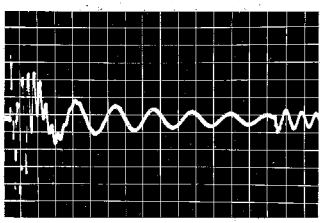

$X_1 = 87.5 \quad f_1 = 15$

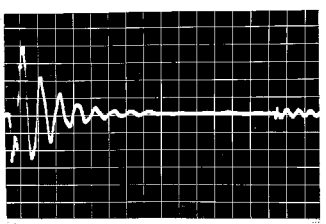

$X_1 = 12.5 \quad f_1 = 10.6$

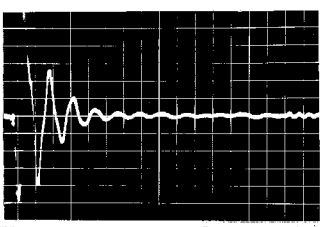

$X_1 = 47.5 \quad f_1 = 10.6$

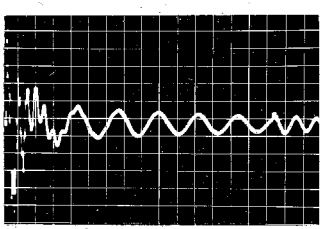

$X_1 = 87.5 \quad f_1 = 10.6$

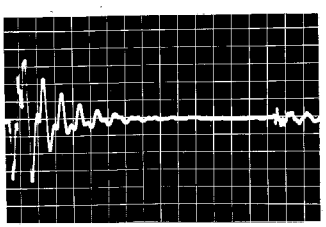

$X_1 = 12.5 \quad f_1 = 7.5$

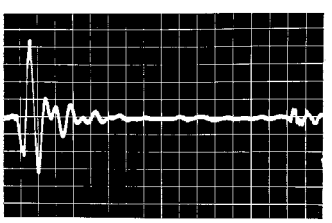

$X_1 = 47.5 \quad f_1 = 7.5$

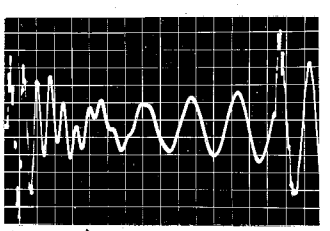

$X_1 = 87.5 \quad f_1 = 7.5$

Shifting Control Surface Location
1sec. = 4.6sqs. K_3H_2 Control

Figure 54

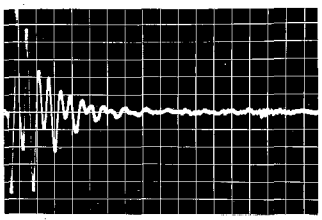

$X_1 = 12.5$ $f_1 = 4.7$

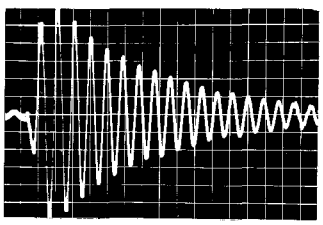

$X_1 = 47.5$ $f_1 = 6.4$

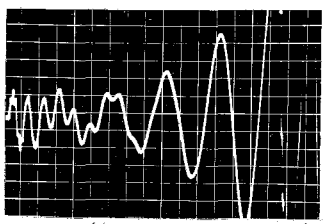

$X_1 = 87.5$ $f_1 = 6.4$

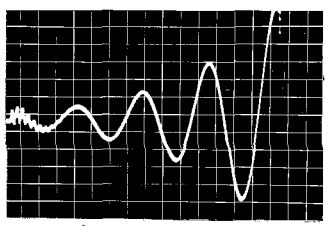

$X_1 = 87.5$ $f_1 = 15$
$k = 0$

Shifting Control Surface Location
1sec. 4.6sqs. K_3H_2 Control

Figure 55

the control surface along the missile affects the behavior of various fuselages structures with the K_3H_2 control. The effect upon system performance is small in all cases except those where the control surface is moved aft of station 75 or those where the fuselage is extremely flexible. With the control surface aft of center the moments of the two airfoils no longer are in opposition, and an unstable low frequency pitching motion is observed.

VII

CONCLUSIONS

The results of this research as discussed in Part VI are a large number of measurements made on an electric model of a simplified but basically complete guided missile. This sort of data provides an adequate foundation for some general conclusions.

The primary objective was to determine how the elasticity of the missile structure influenced the missile performance under feedback control. If elastic deformations are ignored in designing the control, the errors can be very serious. The extent of the error depends upon the flexibility of the elastic structure and the characteristics of the control system. An easy way to describe this dependence is to state that

$$\text{Error} = F\left(\frac{f_1}{f_c}\right) \tag{9}$$

where f_1 is the first bending mode frequency of the fuselage and f_c is the undamped natural frequency of the complete controlled system. The basic nature of the relationship is obvious; the more flexible the structure, the more serious will be the error. It would be fortunate if a simple rule could be established setting a minimum limit for f_1/f_c, such as

$$\frac{f_1}{f_c} \geq 3. \tag{10}$$

The results indicate, however, that the value of such a limit would not be a constant. If the control system is improved by increasing its speed of response it is not sufficient merely to increase the fuselage stiffness until f_1/f_c has the same value. To maintain the same degree of effect due to elasticity the ratio $f_1:f_c$ must be larger if f_c is increased. In the systems studied by the author there was substantially no effect due to elasticity for $f_1/f_c \geq 3$ when f_c was 2.0cps. When f_c was increased to 6.0cps, however, the system performance was seriously affected by the elastic deformation of a fuselage structure which gave an f_1/f_c ratio of 3.5. Thus, it is not possible to specify a single constant or even a curve of values setting an absolute criterion for eliminating the effects of fuselage elasticity. It is only possible to state positively that the effects may be minimized by making f_1/f_c as large as possible, and that whatever decreases may be tolerated in f_c will be of more value than proportional increases in f_1. The author believes that the basic value of $f_1 = 15$cps chosen for this study is too high, and that a value around 10cps is more realistic. This and the fact that newer, faster missiles require faster control systems mean that elasticity effects probably cannot be eliminated but must be compensated for in the system design.

The location of the feedback sensing device is the parameter which specifically couples the elastic behavior of the fuselage with the controlled system performance. This

study has shown that there is a relatively small region of optimum location along the missile length. This region is approximately the twenty-five percent of the missile's length just forward of the midpoint. Clean, fast response may be obtained by locating the sensing device forward of this region at the cost of instability or reduced gain. Locations aft of the center damp the low frequency root very rapidly, but the excitation which such locations provide for an unstable high frequency root is so strong that they seem a poor choice. These effects are increased by a more flexible structure and a faster control system. Two steady state transfer functions are included here (Figures 56 and 57) to show the basis for the observed relation between fuselage rigidity and the effect of sensing point location.

The wide range of parameters involved in a complex aircraft control problem has been pointed out in the literature. (Ref. 3,4) In the course of this investigation some of the possible variations were considered. It is not possible to be specific, but these observations show that flexible fuselage structures also increase the sensitivity of the system to changes in aerodynamic and control parameters, further restricting the designer.

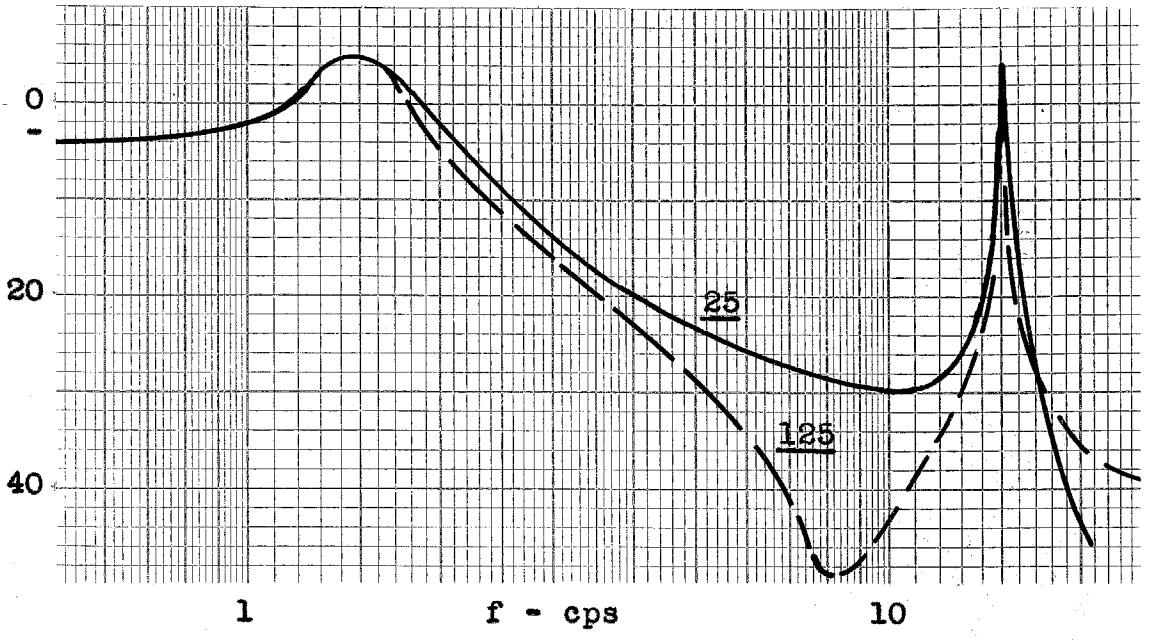

$20\log_{10} G(j\omega)$ $f_1 = 15.0$cps

Figure 56

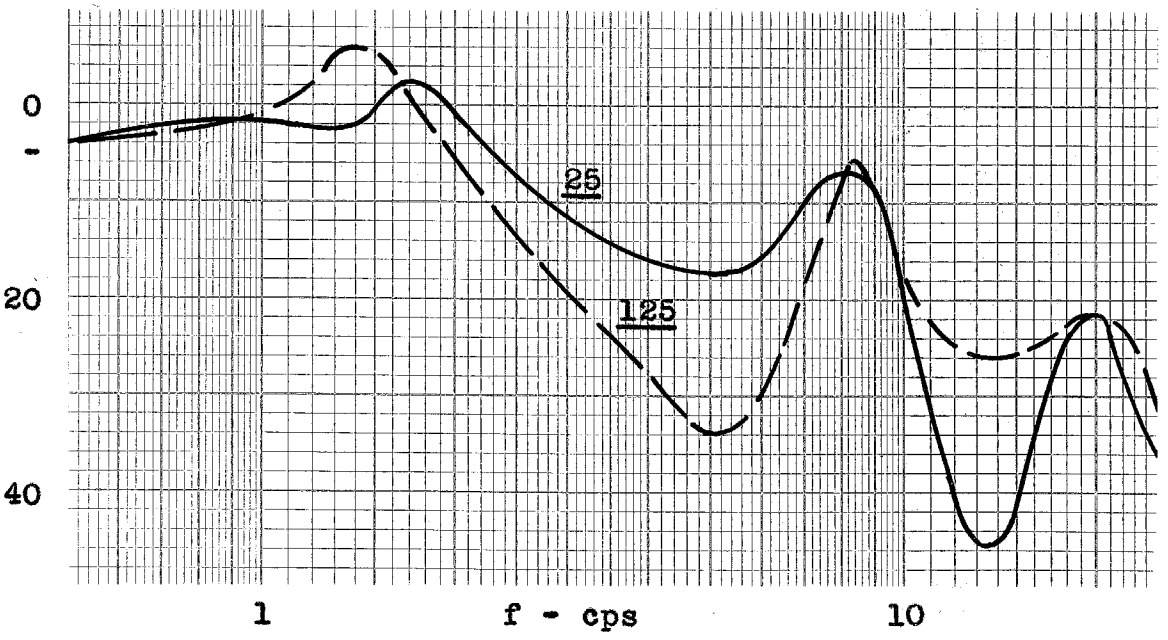

$20\log_{10} G(j\omega)$ $f_1 = 7.5$cps

Figure 57

VIII

REFERENCES

1. R.H. MacNeal, G.D. McCann, C.H. Wilts, "The Solution of Aeroelastic Problems by Means of Electrical Analogies," Journal of the Aeronautical Sciences (December 1951), Vol. 18, No. 12, 777-789.

2. Ibid.

3. William Bollay, "Aerodynamic Stability and Automatic Control," Journal of the Aeronautical Sciences (September 1951), Vol. 18, No. 9, 569-617.

4. Andrew Vazsonyi, "Longitudinal Stability of Autopilot-Controlled Aircraft," NAVORD REPORT 1150 (June 1949).

5. G.D. McCann and R.H. MacNeal, "Beam-Vibration Analysis With the Electric-Analog Computer," Journal of Applied Mechanics (March 1950), Vol. 17, No. 1, p13.

6. Ibid. No. 1.

7. Dana Young and R.P. Felgar Jr, "Tables of Characteristic Functions Representing Normal Modes of Vibration of a Beam," University of Texas Publication No. 4913, (July 1, 1949).

APPENDIX A

The Fuselage Circuit

The derivation of the beam circuit used to represent the missile fuselage in this study is presented in a paper by McCann and MacNeal (Ref. 5). The important equations are repeated here, and complete expressions are given for calculating the values of individual circuit elements.

The behavior of the beam in bending is described by

$$\frac{\partial^2}{\partial x^2}\left\{EI\ \frac{\partial^2 h}{\partial x^2}\right\}+m\ \frac{\partial^2 h}{\partial t^2}=0\ . \tag{11}$$

By defining

$$\theta=\frac{\partial h}{\partial x} \tag{12}$$

and

$$S=\frac{\partial}{\partial x}\left\{EI\ \frac{\partial \theta}{\partial x}\right\}\ , \tag{13}$$

the beam equation becomes

$$\frac{\partial}{\partial x}\ (S)\ +\ m\ \frac{\partial^2 h}{\partial t^2}=0\ . \tag{14}$$

Equations (12), (13), and (14) may be written in finite difference form.

$$\theta_{n+\frac{1}{2}}=\frac{h_{n+1}-h_n}{\Delta x_{n+\frac{1}{2}}} \tag{15}$$

$$\Delta x_{n+\frac{1}{2}}\ S_{n+\frac{1}{2}}=\left\{\theta_{n+3/2}\ -\theta_{n+\frac{1}{2}}\right\}\frac{EI_{n+1}}{\Delta x_{n+1}}+\left\{\theta_{n-\frac{1}{2}}\ -\theta_{n+\frac{1}{2}}\right\}\frac{EI_n}{\Delta x_n} \tag{16}$$

$$\left(S_{n+\frac{1}{2}} - S_{n-\frac{1}{2}}\right) + \Delta x_n m_n \frac{\partial^2 h_n}{\partial t^2} = 0 \qquad (17)$$

The relations between the mechanical and electrical systems are

$$p = \frac{\bar{p}}{N}, \qquad p\theta = -\frac{Kb}{N} E_\theta, \qquad ph = \frac{Ka}{N} E_h, \qquad (18,19,20)$$

$$S = \frac{K}{a} i_s, \quad \text{and} \quad M = -\frac{K}{b} i_m. \qquad (21,22)$$

After substitution of these relationships the finite difference equations become

$$E_{\theta_{n+\frac{1}{2}}} = -\frac{a_o}{b_o \Delta x_{n+\frac{1}{2}}} \left(E_{h_{n+1}} - E_{h_n}\right), \qquad (23)$$

$$-\frac{b_o}{a_o} \Delta x_{n+\frac{1}{2}} i_{s_{n+\frac{1}{2}}} = \frac{b_o^2 V_o^2 EI_{n+1}}{\Delta x_{n+1} V^2 \bar{p}} \left(E_{\theta_{n+3/2}} - E_{\theta_{n+\frac{1}{2}}}\right)$$

$$+ \frac{b_o^2 V_o^2 EI_n}{\Delta x_n V^2 \bar{p}} \left(E_{\theta_{n-\frac{1}{2}}} - E_{\theta_{n+\frac{1}{2}}}\right), \qquad (24)$$

and

$$\left(i_{s_{n+\frac{1}{2}}} - i_{s_{n-\frac{1}{2}}}\right) + \frac{\Delta x_n m_n a_o^2}{N_o^2} \bar{p} E_{h_n} = 0. \qquad (25)$$

Two cells of a circuit which is described by a set of equations similar to (23), (24), and (25), are shown in Figure 58. The circuit equations are

$$E_{\theta_{n+\frac{1}{2}}} T_{n+\frac{1}{2}} = E_{h_{n+1}} - E_{h_n} \qquad (26)$$

across the transformer,

$$- \frac{1}{T_{n+\frac{1}{2}}} i_{s_{n+\frac{1}{2}}} + \frac{1}{\bar{p}L_n} \left(E_{\theta_{n-\frac{1}{2}}} - E_{\theta_{n+\frac{1}{2}}} \right)$$

$$+ \frac{1}{\bar{p}L_{n+1}} \left(E_{\theta_{n+3/2}} - E_{\theta_{n+\frac{1}{2}}} \right) = 0 \qquad (27)$$

at the $n+\frac{1}{2}$ mode in the slope circuit, and

$$i_{s_{n+\frac{1}{2}}} - i_{s_{n-\frac{1}{2}}} + \bar{p}\, C_n\, E_{h_n} = 0 \qquad (28)$$

at the nth mode in the displacement circuit.

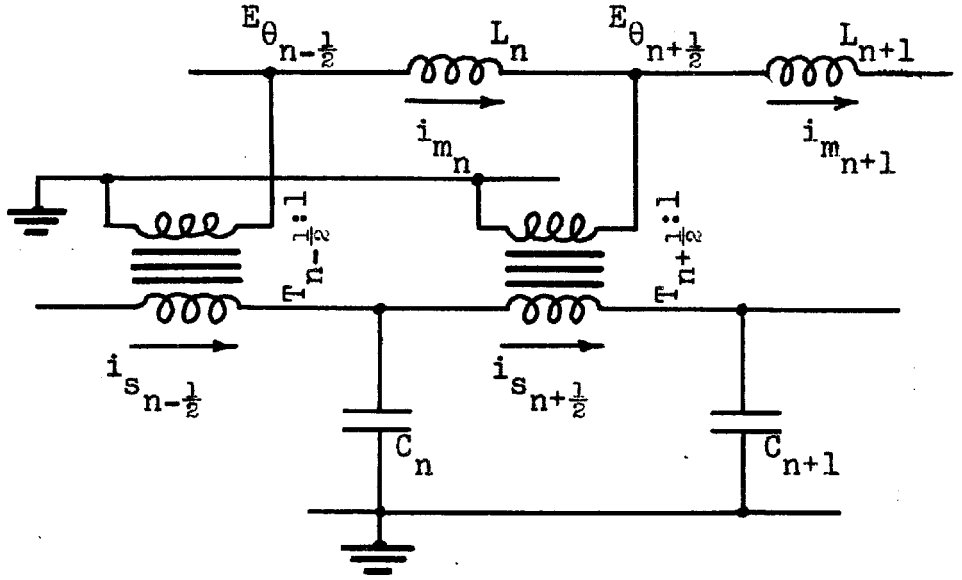

Portion of Typical Beam Circuit
Figure 58

For equivalence between equations (23), (24), and (25) and equations (26), (27), and (28), the circuit elements in Figure 58 must have the values

$$T_{n+\frac{1}{2}} = - \frac{b_o\, \Delta x_{n+\frac{1}{2}}}{a_o} , \qquad (29)$$

$$L_n = \frac{\Delta x_n}{b_o^2 \, EI_n} \left(\frac{V}{V_o}\right)^2 , \tag{30}$$

and

$$C_n = \frac{\Delta x_n \, m_n \, a_o^2}{N_o^2} . \tag{31}$$

The complete fuselage circuit used in this study is shown in Figure 59. For the uniform beam fuselage the values of the numbered circuit elements are

$$C1 \text{ to } C6 = \frac{\Delta x \, m \, a_o^2}{N_o^2} ,$$

$$L1 \text{ to } L4 = \frac{\Delta x}{b_o^2 \, EI} \left(\frac{V}{V_o}\right)^2 ,$$

and

$$T1 \text{ to } T5 = - \frac{b_o}{a_o} \Delta x .$$

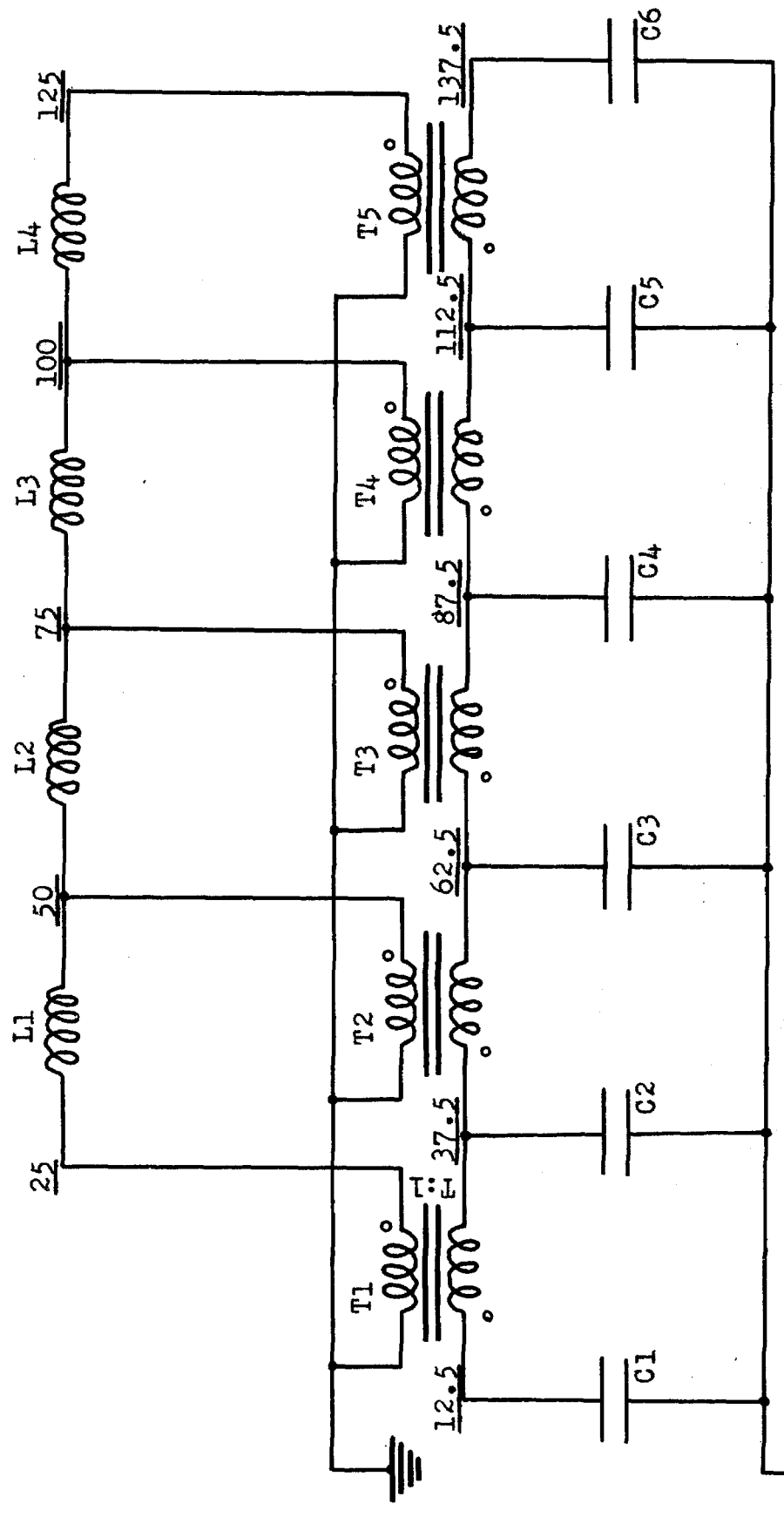

COMPLETE FUSELAGE CIRCUIT
FIGURE 59

APPENDIX B

The Aerodynamic Circuits

1. The Aerodynamic Equations

The original work on electric analogs for aerodynamic forces is described in reference 6. The equations applied to this study are

$$L = -2\pi qS \left[\Psi \left(\frac{cp}{2V}\right) \left(\frac{U}{V}\right) + \frac{c}{4V} p\alpha \right.$$

$$\left. + C \left(\frac{cp}{2V}\right) \left(\frac{ph}{V} + \frac{x_2}{V} p\alpha + \alpha\right) \right] \qquad (32)$$

and

$$Mea = -x_1 L - 2\pi qS \left(\frac{c^2}{8V}\right) p\alpha \, . \qquad (33)$$

Ψ is a lag function for gusts.

C is Theodorsen's function.

Figure 60 shows the airfoil section for which the equations are written.

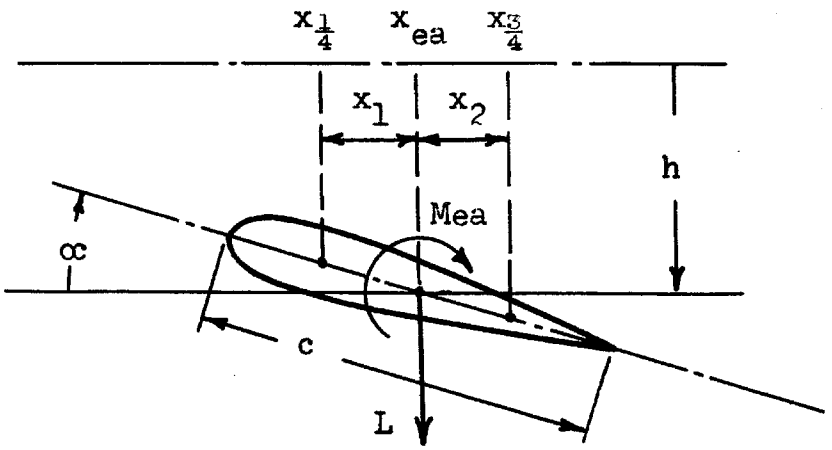

Airfoil Section
Figure 60

The modifications adopted for this study are

1. The gust function is omitted.
2. Theodorsen's function is assumed to be equal to one.
3. The position of the aerodynamic surfaces will be specified by the location of the center of lift, corresponding to the point of insertion of the lift current in the electric model, so that the $x_1 L$ term may be omitted from the moment equation.

With these changes, the equations become

$$L = -2\pi qS \left[\left(\frac{c}{4V} + \frac{x_2}{V}\right)p\alpha + \frac{ph}{V} + \alpha\right] \qquad (34)$$

and

$$Mea = -2\pi qS \left(\frac{c^2}{8V}\right) p\alpha \, . \qquad (35)$$

2. Relating the Mechanical System and the Electric Model

The relations between the mechanical and electrical quantities are

$$p = \frac{\bar{p}}{N} \, , \qquad (36)$$

$$p\alpha = -\frac{Kb}{N} E\alpha \, , \qquad ph = \frac{Ka}{N} E_h \, , \qquad (37,38)$$

$$L = \frac{K}{a} i_h \, , \quad \text{and} \quad Mea = -\frac{K}{b} i_\alpha \, . \qquad (39,40)$$

As described in reference 6, the aerodynamic circuits may be made independent of velocity by choosing

$$N = \frac{N_o V_o}{V} , \tag{41}$$

$$a = \frac{a_o V_o}{V} , \quad \text{and} \quad b = \frac{b_o V_o}{V} , \tag{42,43}$$

where V_o is the reference velocity. When these substitutions are made, the aerodynamic equations become

$$i_h = \frac{2\pi q_o a_o b_o S}{N_o V_o} \left[\left\{ \frac{c}{4} + x_2 + \frac{N_o V_o}{\bar{p}} \right\} E_\alpha - \frac{a_o}{b_o} E_h \right] \tag{44}$$

and

$$i_\alpha = -2\pi q_o S \frac{b_o^2}{N_o V_o} \frac{c^2}{8} E_\alpha . \tag{45}$$

The electric model for the forward aerodynamic circuit is shown in Figure 61. The electrical behavior of the circuit is described by the equations

$$i_{h1} = -A2G1 \left[-\left\{ \frac{R3}{R2} + \frac{1}{\bar{p} R2C10} \right\} E_{\theta 1} + \frac{R4}{R14} E_{h1} + \frac{R4}{R24} E_{\alpha b} + \frac{R4}{R5} E_{\alpha c} \right] \tag{46}$$

and

$$i_{\theta 1} = - \frac{E_{\theta 1}}{R1} . \tag{47}$$

The subscript θ is used now whenever the angle is determined by the slope of the fuselage structure, and α is retained when the symbol represents an additional angle of attack introduced by the control function or by downwash. The $E_{\alpha b}$ and $E_{\alpha c}$ inputs are for the output of the control system and the excitation voltage respectively.

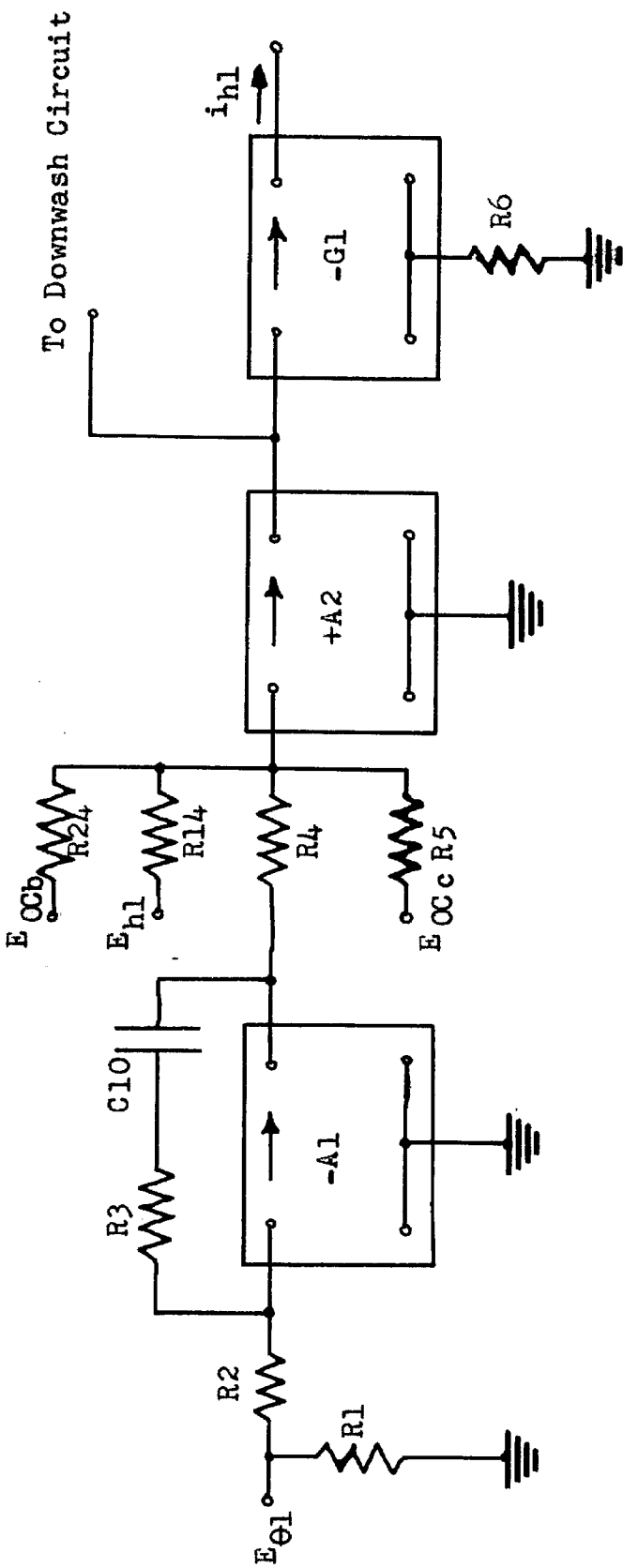

FORWARD AERODYNAMICS CIRCUIT
FIGURE 61

3. Circuit Element Values in the Aerodynamic Circuits

For equations (46) and (47) to be equivalent to equations (44) and (45), the circuit elements must have the values

$$R1 = \frac{8N_o V_o}{2\pi q_o S_1 b_o^2 c_1^2}$$

$$R2 = \frac{A2G1}{2\pi q_o S_1 a_o b_o C10}$$

$$R3 = R2 \frac{2\pi q_o S_1 a_o b_o}{A2G1 N_o V_o} \left(\frac{c_1}{4} + x_{21}\right)$$

R4 = 20K Arbitrary value

R5 = 200K Arbitrary value

R6 = 500 Arbitrary value

$$R14 = R4 \frac{A2G1 N_o V_o}{2\pi q_o S_1 a_o^2}$$

R24 = R5

C10 = 0.1 Arbitrary value

$$G1 = \frac{1}{R6}$$

A2 = 5.0 Arbitrary value.

The values of R1 and R8 in the tail circuit are so large that they do not affect the solutions, and in practice they were omitted. The aerodynamic circuit for the tail surface is similar in every respect, except that an input terminal

is provided for $E_{\alpha d}$, the downwash voltage, instead of $E_{\alpha b}$. The complete tail circuit and the interconnection of the aerodynamic circuits with the fuselage and control circuits are shown on the complete circuit diagram, Figure 71. The values of the circuit elements in the tail aerodynamic circuit are

$$R8 = \frac{8N_oV_o}{2\pi q_o S_2 b_o^2 c_2^2}$$

$$R9 = \frac{A5G2}{2\pi q_o S_2 a_o b_o C11}$$

$$R10 = R9 \frac{2\pi q_o S_2 a_o b_o}{A5G2\ N_o V_o} \left(\frac{c_2}{4} + x_{22}\right)$$

R11 = 20K Arbitrary value

R12 = 500K Arbitrary value

R13 = 500 Arbitrary value

$$R15 = R11 \frac{A5G2\ N_oV_o}{2\pi q_o S_2 a_o^2}$$

R25 = R5

C11 = 0.1 Arbitrary value

$G2 = \frac{1}{R13}$

A5 = A2 Arbitrary value

4. The Downwash Circuit

To account for downwash in the electric model a voltage, $E_{\alpha d}$, proportional to the lift on the forward aerodynamic surface, is added to the angle of attack voltage in the tail circuit. The downwash delay time is simulated by an electrical delay line. The circuit used is shown in Figure 62. The delay time of such a network is

$$\Delta\bar{t} = n\sqrt{LC}\ , \tag{48}$$

where n (three in this study) is the number of T sections and L is the total inductance per section.

If D is the distance between the two airfoils,

$$\Delta t = \frac{D}{V}\ , \tag{49}$$

and

$$\Delta\bar{t} = \frac{D}{NV}\ , \tag{50}$$

or

$$\sqrt{LC} = \frac{D}{3N_oV_o}\ . \tag{51}$$

Choosing approximately equal values of L and C which satisfy equation (51), the circuit elements in Figure 62 are specified by

$$L5 = \frac{L}{2}$$

$$L6 = L$$

$$L7 = L$$

$$L8 = \frac{L}{2}$$

$$C7 = C$$

$$C8 = C$$

$$C9 = C$$

$$R7 = \sqrt{\frac{L}{C}}$$

The gain of A3 is adjusted to obtain the desired downwash ratio between the output of A2 in the forward circuit and the related output of A5 in the tail circuit. A3 must be negative to produce lift current, i_{h2}, of the proper sign at the output of G2.

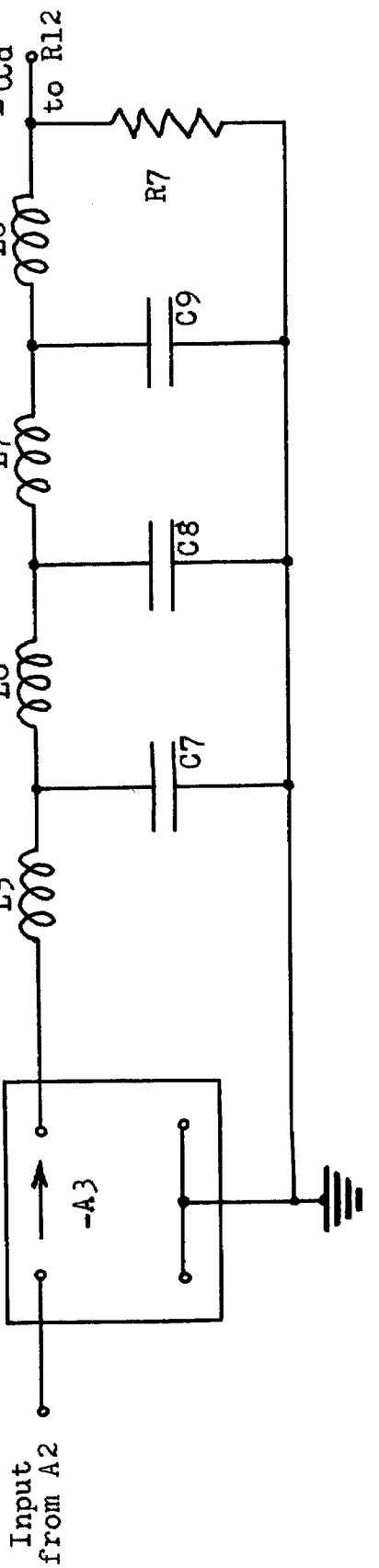

DOWNWASH CIRCUIT
FIGURE 62

APPENDIX C

The Control Circuit

The control system assumed for this study, a second order system with position and rate feedback, is described by

$$\alpha_b = -K \frac{(1+rp)}{(1+\tau 1p)(1+\tau 2p)} \theta_s \cdot \tag{52}$$

The complete control circuit model is shown in Figure 63. The behavior of this circuit is described by

$$E_{\alpha b} = \frac{A7A8\left(\frac{R21}{R20} + \frac{1}{p}\frac{1}{R20C14}\right)}{(1+R22C15p)(1+R23C16p)} E_{\theta s} \cdot \tag{53}$$

It is known that

$$E_{\theta s} = -\frac{N}{Kb} p\theta_s \cdot \tag{54}$$

Except for a very small term, due to R3 in the feedback loop of A1 (See Figure 61 in Appendix B), the voltage E at the input to R4 is related to the fuselage slope angle at the forward aerodynamic surface by

$$E = -E_\theta \frac{1}{p}\frac{1}{R2C10} \tag{55}$$

and

$$E_\theta = -\frac{N}{Kb} p\theta \cdot \tag{56}$$

Combining (55) and (56),

$$E = \frac{\theta}{KbR2C10} \cdot \tag{57}$$

Since the gain through R24 is one-tenth of the gain through R4, the relationship between $E_{\alpha b}$ and the equivalent control surface angle, α_b, is

$$E_{\alpha b} = \frac{10\alpha_b}{KbR2C10} \tag{58}$$

Substituting equations (54) and (58) into (53), the relation between θ_s and α_b is given in terms of the electric model circuit elements as

$$\alpha_b = \frac{-A7A8R2C10\ (1+pNR21C14)}{10R20C14\ (1+R22C15Np)(1+R23C16Np)}\ \theta_s \tag{59}$$

Equations (52) and (59) must be identical if the electric model is to represent the physical system. To meet this requirement the circuit elements must have the values

R2 = 530K (See Appendix B)

C10 = 0.1 (See Appendix B)

R20 = 100K Arbitrary value

C14 = 0.5 to 3.0 Arbitrary values

C15 = 0.5 Arbitrary value

C16 = 0.5 Arbitrary value

$$R21 = \frac{r}{C14N}$$

$$R22 = \frac{\tau 1}{C15N}$$

$$R23 = \frac{\tau 2}{C16N}$$

$$A7A8 = K\ \frac{10R20C14}{R2C10}$$

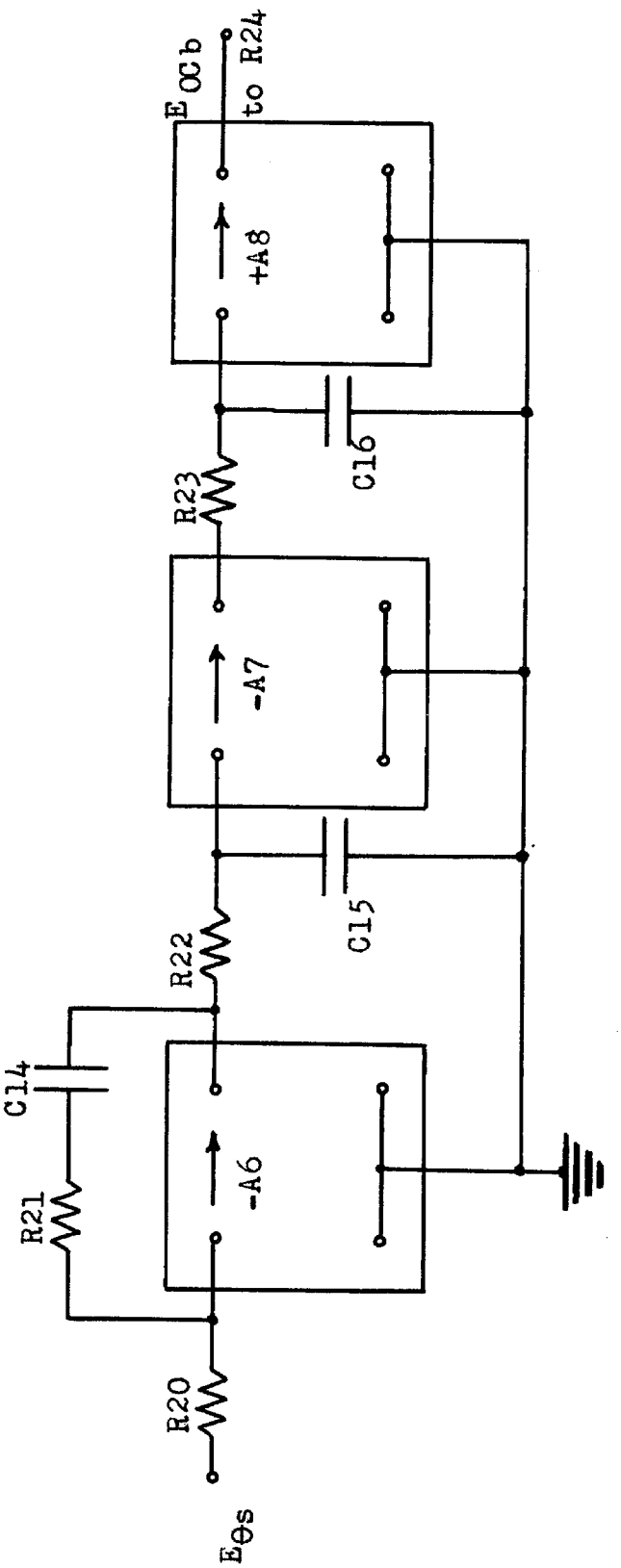

CONTROL SYSTEM CIRCUIT
FIGURE 63

APPENDIX D

Mode Check of the Fuselage Circuit

In the progressive assembly of the electric model it is important to check the accuracy of the circuits at various stages. The first complete circuit upon which tests may be conveniently made is the electric model of the fuselage beam. The accuracy of this circuit as a representation of the missile fuselage beam is readily evaluated by comparison of theoretical mode shapes and frequencies with those measured on the electric model.

Figures (64), (65), and (66) present such comparative data for the first three modes of the reference condition fuselage beam. This is a uniform beam with W = 750 pounds and f_1 = 15.0 cps. The tables of Young and Felgar (Ref. 7) were used to obtain the theoretical mode shapes and frequencies. The measured data was obtained from voltage measurements at the nodes of the displacement circuit and frequencies corresponding to minimum current input from the source used to excite the electric model.

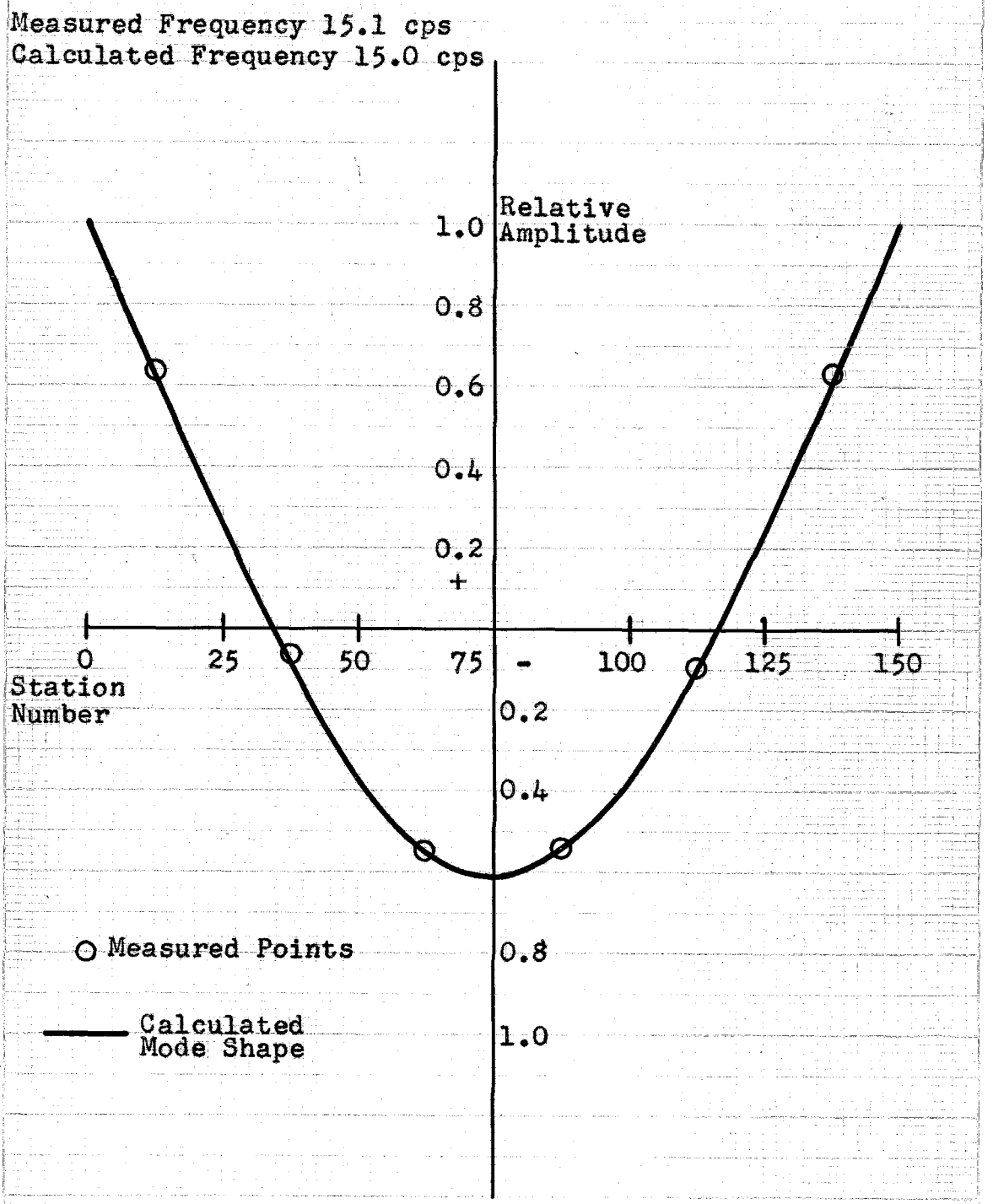

MODE STUDY OF FUSELAGE BEAM
1st MODE - REFERENCE CONDITIONS
FIGURE 64

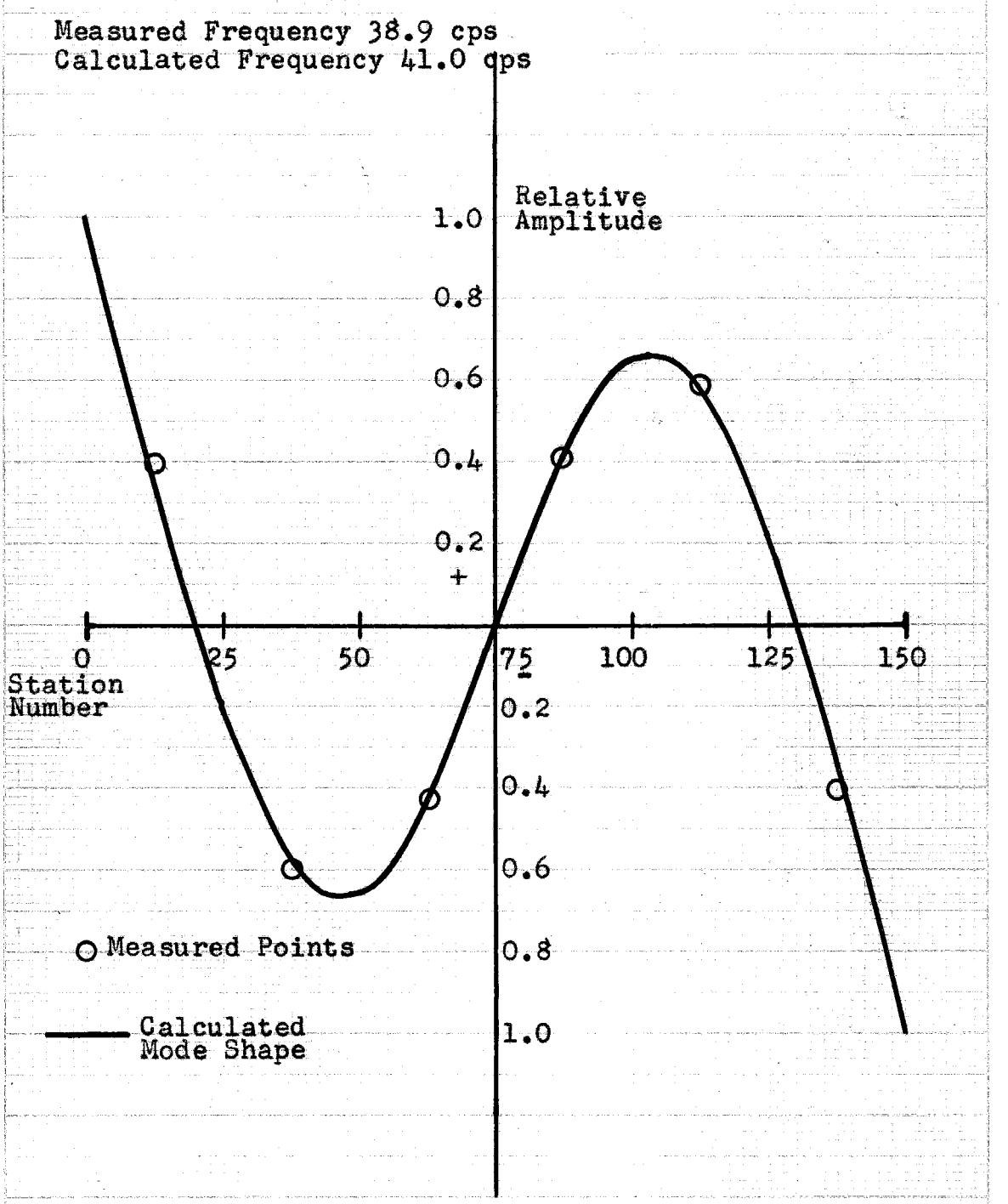

MODE STUDY OF FUSELAGE BEAM
2nd MODE - REFERENCE CONDITIONS
FIGURE 65

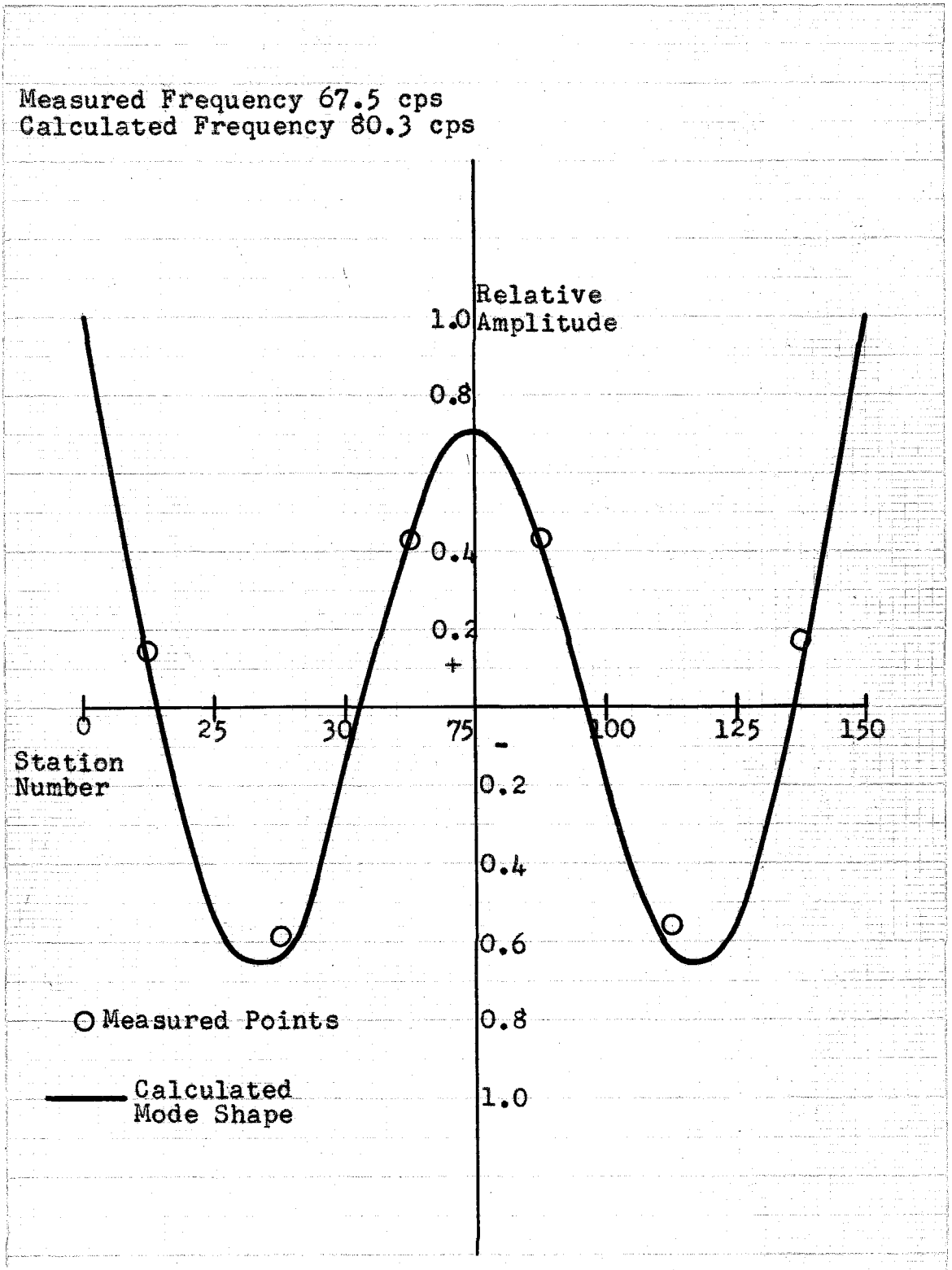

MODE STUDY OF FUSELAGE BEAM
3rd MODE - REFERENCE CONDITIONS
FIGURE 66

APPENDIX E

System Check by Steady State Data

Before introducing the control circuit, a large number of steady state measurements were made to determine the transfer function, including aerodynamic effects, between control surface position and the slope angle at various stations along the fuselage. This form of data was discarded in favor of oscillographic transient response records when the complexity of the problem became more apparent. However, some of the steady state data was used to predict the behavior of the complete closed loop system and thus provide another check on the formulation of the electric model circuits.

In particular, Figure 67 shows the transfer function, $G(j\omega)$, measured between control surface angle, α_c, and fuselage slope angle, θ_s, at station 50 under reference conditions. This plot was obtained from measured values of the voltages $E_{\alpha c}$ at R5 and $E_{\theta s}$ at station 50 in the fuselage slope circuit when the combined fuselage and aerodynamic circuits were excited by a variable frequency sinusoidal voltage applied at R5.

One of the basic electrical to mechanical conversions is

$$E_{\theta s} = - \frac{N}{Kb} p \theta_s \qquad (60)$$

Since R5 = R24, the equation derived for $E_{\alpha b}$ in Appendix C applies also to $E_{\alpha c}$.

$$E_{\alpha c} = \frac{10\alpha_c}{Kb\ R2C10} \tag{61}$$

Combining equations (60) and (61),

$$G(p) = \frac{\theta_s}{\alpha_c} = -\frac{10}{p\ R2C10}\ \frac{E_{\theta s}}{E_{\alpha c}}\ , \tag{62}$$

and, for the steady state,

$$G(j\omega) = +j\ \frac{10}{\omega\ R2C10}\ \frac{E_{\theta s}}{E_{\alpha c}}\ . \tag{63}$$

The amplitude and phase of $E_{\theta s}/E_{\alpha c}$ were determined by measurements on the electric model. Application of equation (63) produced data for the plot of $G(j\omega)$ in Figure 67.

The basic equation for the control system is

$$\alpha_b = KH(p)\ \theta_s \tag{64}$$

where

$$H(p) = \frac{(1+rp)}{(1+\tau 1p)(1+\tau 2p)}\ . \tag{65}$$

Figure 68 is a plot of the gain and phase of $\frac{(1+0.3p)}{(1+0.1p)^2}$, the reference condition form of H(p). The complete control system transfer function is obtained by shifting the gain scale in accordance with the value of $20 \log_{10} K$.

The combined transfer function $G(j\omega)H(j\omega)$, obtained from Figures 67 and 68 is plotted in Figure 69. The gain margin and frequency at 180° phase shift are -1.5 db and 2.0 cps. The complete system should be marginally stable at 2.0 cps when the value of K is 0.84. The transient response of this same system,

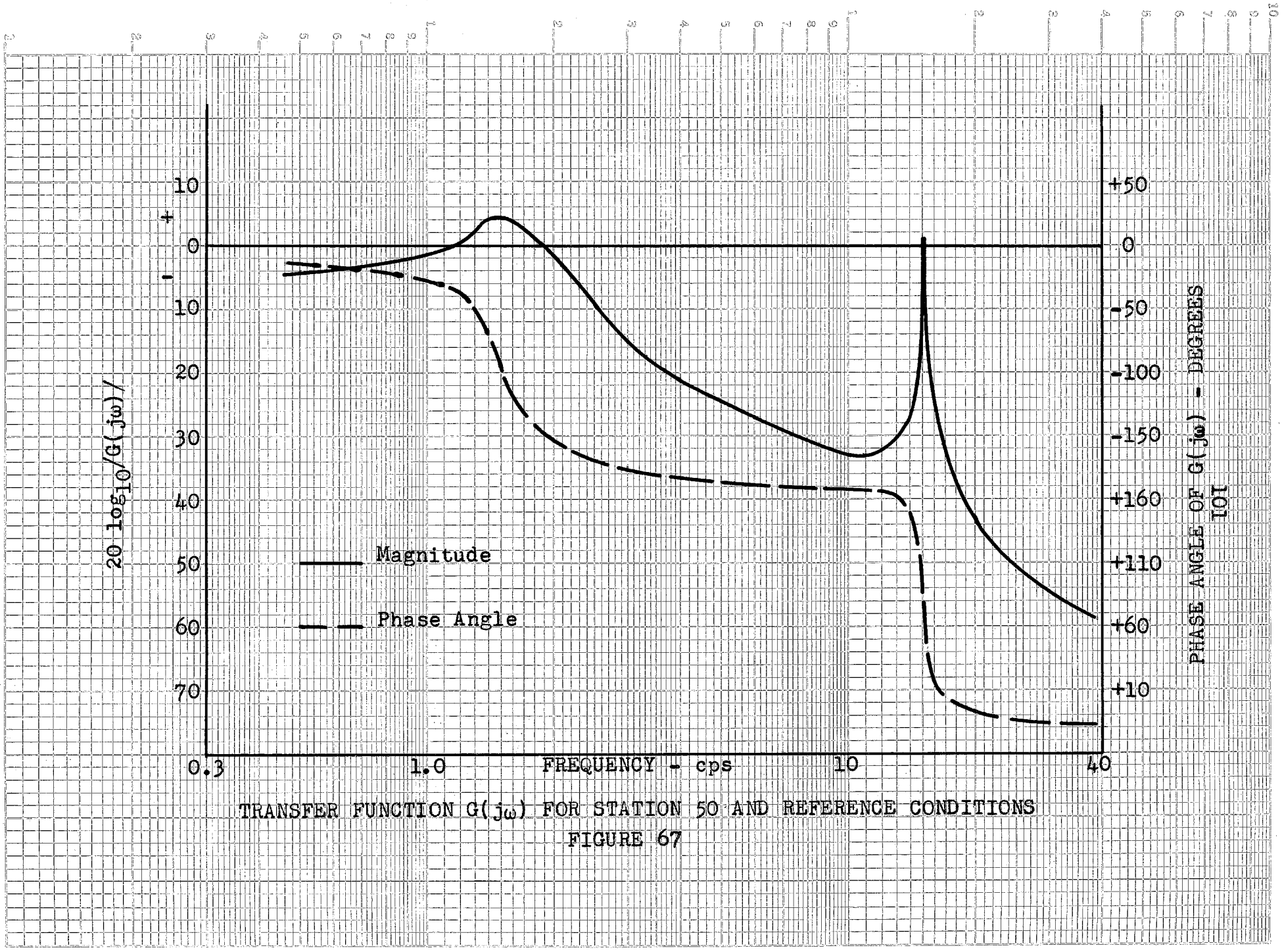

TRANSFER FUNCTION G(jω) FOR STATION 50 AND REFERENCE CONDITIONS

FIGURE 67

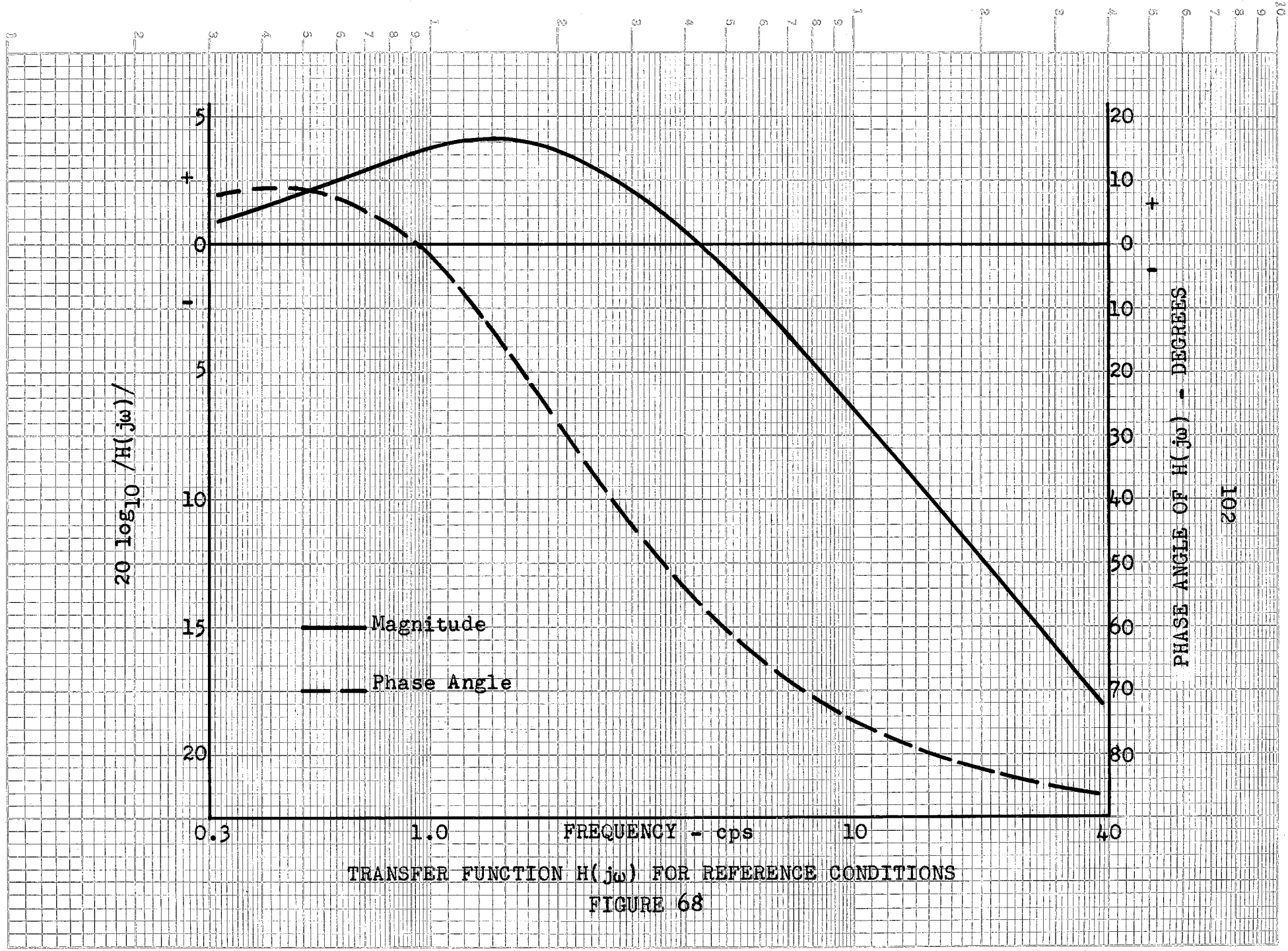

TRANSFER FUNCTION H(jω) FOR REFERENCE CONDITIONS

FIGURE 68

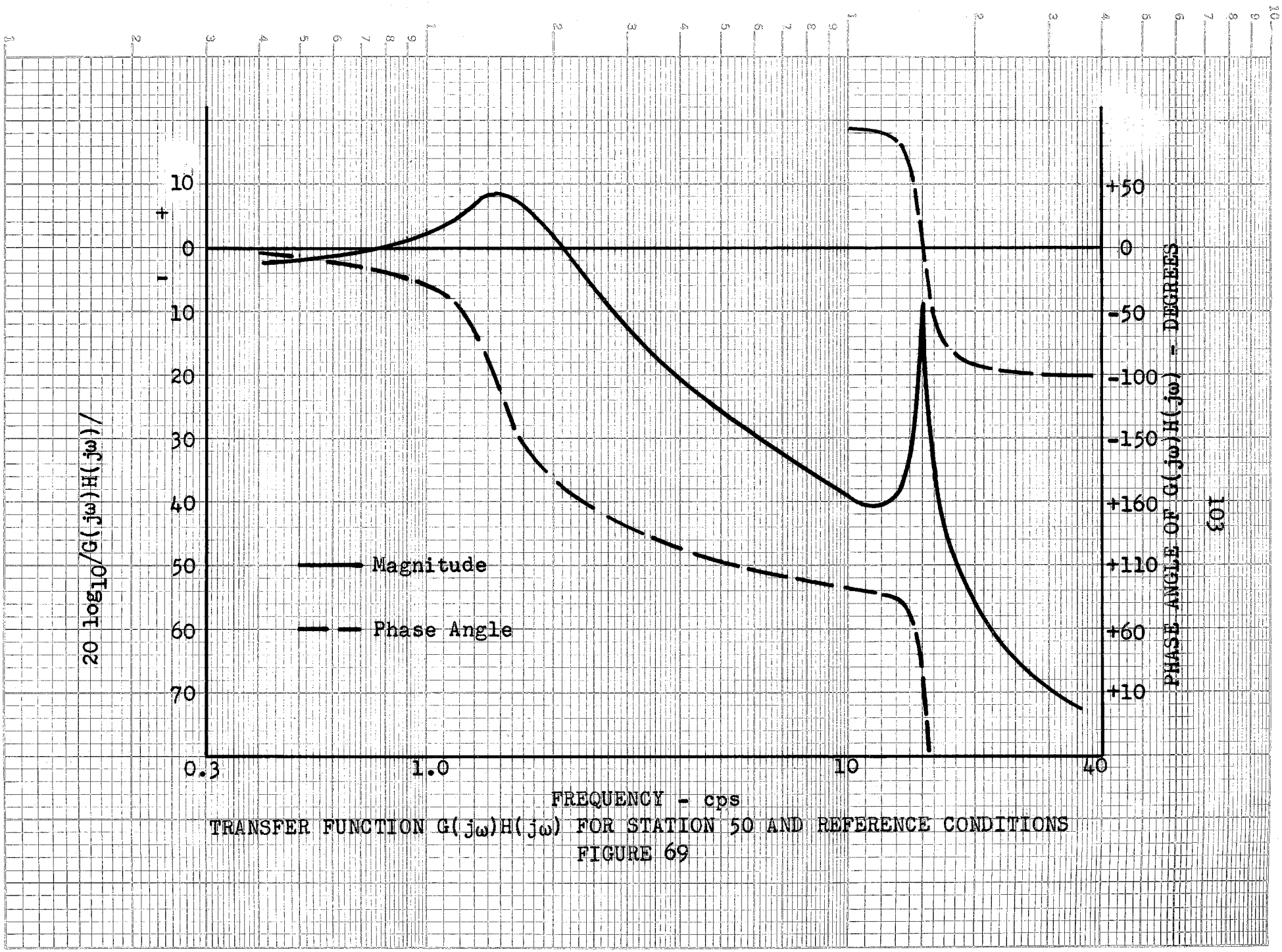

TRANSFER FUNCTION $G(j\omega)H(j\omega)$ FOR STATION 50 AND REFERENCE CONDITIONS

FIGURE 69

with K = 0.9, is shown in the oscillograph of Figure 70. The frequency of this response is 1.95 cps.

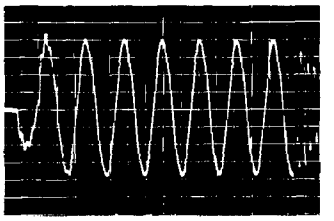

1sec. = 4.1sqs.
Transient Response
Reference Condition System
Figure 70

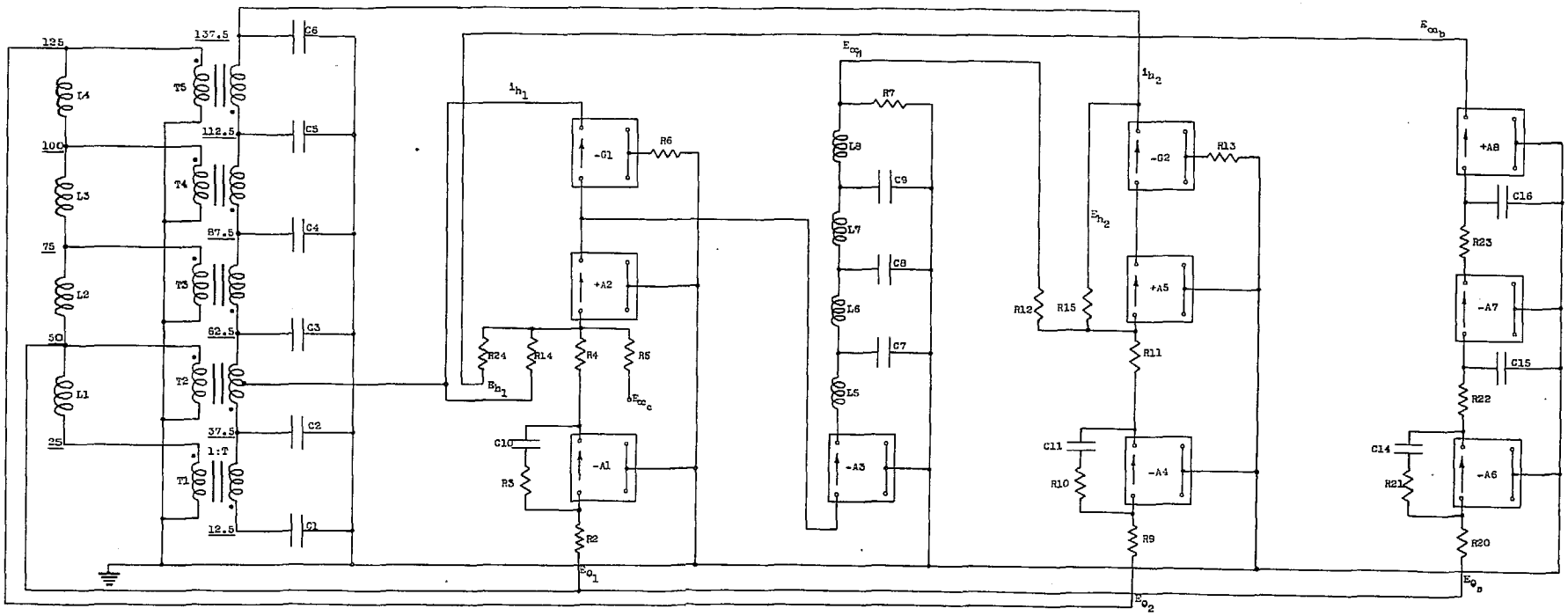

Complete Electric Model

Figure 71